UNIVERSIDADE DA BEIRA INTERIOR
Ciências da Saúde

Desenvolvimento de nanopartículas inorgânicas para aplicações terapêuticas

Diana Rodrigues Dias

Dissertação para obtenção do Grau de Mestre em
Ciências Biomédicas
(2º ciclo de estudos)

Orientador: Prof. Doutor Ilídio Joaquim Sobreira Correia
Co-orientador: Mestre André Ferreira Moreira

Covilhã, outubro de 2016

Aos meus eternos companheiros:

avós, mãe, pai e mana…

"A ciência investiga;
A religião interpreta;
A ciência dá ao Homem conhecimento, que é poder;
A religião dá ao Homem sabedoria, que é controlo;
A ciência lida principalmente com factos;
A religião lida principalmente com valores;
Os dois não são rivais, são complementares."

Martin Luther King Jr

Acknowledgements

Firstly, I would like to thank my supervisor Professor Ilídio Correia, for the opportunity to work with him and integrate his group. His assistance and constant feedback contributed to my progress during this thesis. I am also grateful for all recommendations, guidance and exigency, which were crucial to make me grow up as a professionally.

I would also like to thank my co-supervisor, André Moreira, for all the help, tireless patience and the time he spent with me. Our constant work discussions contributed for the development of my lab skills. Without his assistance and encouragement this work could not be accomplished.

I thank Professor Abílio Silva for the support in the acquisition of the porosimetry data. Additionally, I also thank Dr. Ana Paula for the help in the acquisition of transmission electron microscopy images.

Moreover, I would like to show my gratitude to my lab colleagues for their friendship and principally, for their infinite good vibes. Specially, I am so grateful to Cleide for her unlimited incentive and all the help in my doubts.

To my friends, I would like to demonstrate my honest acknowledgments for their continuous encouragement and force in worst moments. Particularly, I am so grateful to my girls, Marta, Sandra and Tânia for always listening to my confidences and for their unlimited patience and friendship.

My sincere thanks to my parents, Natalina and Virgílio, my little sister Daniela and my grandmother Maria, for all the patience, comprehension and encouragement even in ways unknown to them. Without their continuous support, none of this would be possible. Lastly, I would like to thank Duarte for being my constant support, for his patience and encouragement in my difficulties. My words are not enough to thank for his unconditional love.

Finally, thank you God.

Resumo

Na atualidade, o cancro é uma das principais causas de morte da população mundial e para a qual os tratamentos disponíveis demonstram uma ineficácia relativa. Devido a este cenário alarmante, a aplicação da Nanotecnologia na área do cancro tem vindo a crescer a fim de melhorar o diagnóstico e as taxas de sobrevivência associados a esta patologia. Nesta área, as nanopartículas constituem uma abordagem promissora, uma vez que são capazes de prevenir a interação dos fármacos quimioterapêuticos com os tecidos saudáveis. Por outro lado, as nanopartículas previnem ainda a degradação prematura dos fármacos quimioterapêuticos. De entre os vários materiais estudados, as nanopartículas de ouro revestidas com sílica mesoporosa têm mostrado ser estruturas promissoras para a aplicação na terapia do cancro. Contudo, o estudo da influência da morfologia da partícula no desempenho biológico das nanopartículas de ouro revestidas com sílica mesoporosa ainda foi pouco explorado até ao momento.

Na presente tese foram produzidas nanopartículas de ouro com um revestimento de sílica mesoporosa (Au-MSSs), com forma esférica ou de bastonete, com o objetivo de estudar o efeito da morfologia na encapsulação e perfil de libertação de um determinado fármaco, biocompatibilidade, internalização celular e citotoxicidade das nanopartículas. Os resultados obtidos demonstraram que ambos os tipos de nanopartículas possuem tamanhos ideais (<200 nm) para a sua possível acumulação passiva no tecido tumoral. Para além disto, as propriedades óticas das Au-MSS em forma de bastonete permitem a sua aplicação na terapia fototermal. Por outro lado, as nanopartículas esféricas apresentaram uma melhor eficiência de encapsulação da doxorrubicina (80%), quando comparadas com as nanopartículas em forma de bastonete (52%). Apesar da menor quantidade de doxorrubicina encapsulada pelas Au-MSS em forma de bastonete, estas têm a capacidade de entregar uma maior quantidade de fármaco às células cancerígenas, devido à sua maior internalização pelas células cancerígenas. Por outro lado, os resultados obtidos *in vitro* revelaram que ambos os tipos de nanopartículas possuem um efeito citotóxico superior ao da doxorrubicina na sua forma livre. Adicionalmente, as nanopartículas em forma de bastonete quando irradiadas com luz de comprimento de onda próximo do infravermelho produziram um maior efeito citotóxico, o que resulta da sua capacidade de combinar a abordagem de quimioterapia (entrega de doxorrubicina) e de terapia fototermal (produção de calor após irradiação com luz de comprimento de onda próximo do infravermelho).

Em suma, neste trabalho foi feito o primeiro estudo comparativo entre Au-MSS com diferentes morfologias, tendo-se verificado que este parâmetro influencia as propriedades terapêuticas apresentadas pelas partículas. A versatilidade apresentada por estes sistemas permite postular a sua futura aplicação no tratamento de diferentes doenças que afetam o ser humano.

Palavras-Chave

Ouro, Sílica, Morfologia da Nanopartícula, Terapia do Cancro, Radiação Próxima do Infravermelho

Resumo Alargado

Na atualidade, o cancro é uma das doenças com maior impacto na saúde pública a nível mundial. As elevadas taxas de incidência e de mortalidade associadas a esta doença devem-se, em grande parte, à falta de eficácia dos tratamentos atualmente usados em meio clínico, como a radioterapia, cirurgia e quimioterapia. A quimioterapia é a abordagem terapêutica mais utilizada na clínica, no entanto esta apresenta diversas desvantagens relacionadas com a falta de especificidade e rápida degradação dos fármacos quimioterapêuticos, o que leva a que estes agentes tenham uma baixa biodisponibilidade. Devido a este facto, são administradas doses elevadas de fármacos aos pacientes, o que na maioria dos casos, tem efeitos secundários. Este cenário evidência a necessidade de desenvolver novas abordagens terapêuticas para o cancro.

Neste contexto, os avanços na área da Nanotecnologia têm permitido a construção de sistemas à escala nanométrica (nanopartículas), que superam algumas das limitações dos tratamentos atualmente disponíveis na clínica. De um modo geral, uma das principais vantagens dos nanotransportadores está associada à sua capacidade de se acumularem preferencialmente no tumor. Além disto, durante a circulação na corrente sanguínea, os nanotransportadores são capazes de proteger, transportar e controlar a libertação dos fármacos, diminuindo a sua interação com os tecidos saudáveis e, por outro lado, incrementar o seu efeito terapêutico. Dentro do vasto leque de nanopartículas em desenvolvimento, as nanopartículas de ouro revestidas com sílica mesoporosa têm sido intensamente estudadas para aplicação na área do cancro. De uma forma geral, esta combinação de materiais permite a construção de nanopartículas multifuncionais, em que o revestimento de sílica mesoporosa permite a encapsulação e transporte de fármacos, conferindo proteção aos agentes quimioterapêuticos e possibilitando a sua entrega no local alvo. Por sua vez, o núcleo de ouro pode ser usado como agente fototermal, isto é, estas nanopartículas têm a capacidade de converter a radiação proveniente de uma fonte de luz em calor, o qual pode exercer um efeito citotóxico nas células cancerígenas. Para além disto, este aumento local de temperatura pode sensibilizar as células cancerígenas para a ação dos fármacos (termosensibilização), potenciando o seu efeito terapêutico. Adicionalmente, as nanopartículas de ouro podem ainda atuar como agentes de imagiologia, possibilitando a deteção de massas tumorais ou a monitorização da eficácia terapêutica através de tomografia computorizada ou ressonância magnética.

Para além da escolha do tipo de nanopartícula a aplicar na terapia do cancro, o design destas é igualmente um fator preponderante para a sua eficácia. O tamanho, a carga, a composição de superfície e a morfologia são parâmetros que devem ser investigados, pois influenciam a forma como as partículas interagem com o corpo humano durante a sua circulação na corrente sanguínea, bem como com as células (biocompatibilidade e internalização). Em particular, a

influência da morfologia da nanopartícula é um parâmetro ainda pouco estudado e sobre o qual os resultados obtidos são contraditórios, existindo assim a necessidade de aprofundar o conhecimento do efeito da morfologia das nanopartículas na sua aplicação para fins terapêuticos.

Na presente tese foi efetuado um estudo comparativo entre dois tipos de nanopartículas compostas por um núcleo de ouro e um revestimento de sílica mesoporosa (Au-MSS), com forma de esferas ou bastonetes, com o intuito de discutir o efeito da morfologia na encapsulação e perfil de libertação de um determinado fármaco, biocompatibilidade, internalização celular e citotoxicidade das nanopartículas. As nanopartículas Au-MSS esféricas produzidas apresentaram um tamanho de 109 nm e os bastonetes 70 x 47 nm (comprimento x largura). Estes valores encontram-se dentro do intervalo de valores considerado ideal para a aplicação intravenosa das partículas e, posteriormente, permitir a sua acumulação passiva no tumor. Por outro lado, verificou-se que estes nanotransportadores são capazes de armazenar um fármaco quimioterapêutico (doxorrubicina) no seu interior. As Au-MSS esféricas mostraram uma maior capacidade para encapsular a doxorrubicina, apresentando uma eficiência de encapsulação para este fármaco na ordem dos 80%, enquanto os bastonetes apenas encapsularam 52% da doxorrubicina. Este resultado é explicado pelo maior volume de poro exibido pelas Au-MSS esféricas. Adicionalmente, devido às diferenças na forma do núcleo de ouro, os bastonetes apresentaram dois picos de absorção distintos no espectro de ultravioleta-visível, a 500 e 770 nm, enquanto as nanopartículas esféricas apenas apresentam um pico a 550 nm. Esta particularidade das Au-MSS com forma de bastonetes permite que estas sejam aplicadas na terapia fototermal, uma vez que quando expostas a radiação eletromagnética com comprimento de onda próximo do infravermelho estes libertam energia sobre a forma de calor, o que leva a um aumento de temperatura (efeito fototermal).

Os testes *in vitro* realizado com células cancerígenas demonstraram que ambos os nanosistemas são internalizados com eficiência. Contudo, verificou-se que os bastonetes conseguiram entregar uma maior quantidade de doxorrubicina às células cancerígenas, o que indica que estes apresentam uma maior eficácia de internalização nas células cancerígenas do que as partículas esféricas. Nos estudos de citotoxicidade, verificou-se que ambas as Au-MSS contendo doxorrubicina apresentaram um efeito terapêutico superior ao resultante da ação da doxorrubicina na sua forma livre. Além disso, quando irradiados com uma radiação próxima do infravermelho (808 nm, 1.7 W/cm^2, 5 min), os bastonetes contendo doxorrubicina apresentaram um maior efeito citotóxico do que as Au-MSS esféricas. Este resultado indica que os bastonetes são capazes de conjugar a ação terapêutica do fármaco com a ação fototermal, o que permite incrementar o seu efeito terapêutico.

Em suma, a morfologia das Au-MSS revelou-se ter importância sobre as propriedades físico-químicas e biológicas apresentadas pelas partículas. Além disso, a versatilidade que estes

sistemas apresentam permite que, dependendo da aplicação desejada, os sistemas possam ser produzidos com diferentes formas, de acordo com o tipo de patologia que se pretende tratar.

Abstract

Nowadays, cancer is a leading cause of mortality among the worldwide population, for which the currently available treatments display a limited efficacy. Chemotherapy, the main therapeutic approach used for the treatment of this disease, has a sub-optimal effect due to the weak selectivity for cancer cells and rapid degradation of chemotherapeutic agents. Motivated by this alarming scenario, Nanotechnology applied to cancer-related topics has been growing for improving cancer diagnosis and survival rates. In this field, the design of nanoparticles is a promising approach, since these platforms can provide protection to drugs and decrease their interaction with healthy tissues. Among the several materials studied, gold nanoparticles with a mesoporous silica shell are promising hybrid nanostructures for cancer therapy.

In this thesis, nanoparticles composed of a gold core and a silica shell (Au-MSSs) with spherical or rod-like shape were produced, in order to disclose the effect of nanomaterials shape on the nanoparticle properties, such as their drug loading capacity and release profile, biocompatibility, cellular uptake and cytotoxic effect towards cancer cells. Both Au-MSS nanoparticles showed adequate sizes for a possible passive accumulation in tumor tissues. Moreover, the optical properties displayed by Au-MSS rods allowed their application in photothermal therapy. Furthermore, the spherical nanoparticles presented an improved Dox drug encapsulation efficiency (80%) when compared to that of rod-shaped (52%). However, despite the lower Dox loaded in the Au-MSS rods, these particles delivered a higher quantity of drug to cancer cells, which indicates that Au-MSS rods are more uptaken by cancer cells. In addition, the *in vitro* experiments also revealed that both Au-MSSs demonstrated a higher cytotoxic effect against cancer cells than free Dox, which is crucial for cancer therapy. Moreover, the Dox loaded rod-shaped nanoparticles irradiated with near-infrared light produced an increased therapeutic effect on cancer cells, when compared to the spherical particles, which results from the rods capacity to combine chemo- and photothermal therapeutic actions.

In summary, the results presented in this thesis confirm the effect of nanoparticle shape on its performance on cancer therapy. Further, depending on the desired application, the shape and the type of nanoparticle should be taken into account towards the development of a more personalized and effective therapy.

Keywords

Gold, Silica, nanoparticle shape, NIR, cancer therapy

List of Publications

Articles in peer reviewed international journals:

Moreira, A. F., Dias, D. R., and Correia, I. J. (2016). "Stimuli-responsive mesoporous silica nanoparticles for cancer therapy: A review." Microporous and Mesoporous Materials. 236: 141-157. (Available on: http://dx.doi.org/10.1016/j.micromeso.2016.08.038)

Dias, D. R., Moreira, A. F., and Correia, I. J. "Comparative study of the effect gold nanoparticles coated with mesoporous silica shape on its biological performance." Journal of Materials Chemistry B (4.872), under review.

Moreira, A. F., Dias, D. R., Costa E. C., and Correia, I. J. "Thermo- and pH-Responsive Nano-in-Micro Particles for Combinatorial Drug Delivery to Cancer Cells." Colloids and Surfaces B: Biointerfaces (3.902), under review.

Poster communications:

Dias, D. R., Moreira, A. F., and Correia, I. J. "Synthesis and characterization of gold nanoparticles coated with mesoporous silica", V Encontro Nacional de Estudantes de Materiais (ENEM), 29th of September, Universidade da Beira Interior, Covilhã, Portugal.

Index

Figure Index

Table Index

List of Abbreviations

ABC	ATP-binding cassette
ANOVA	One-way analysis of variance
ATP	Adenosine triphosphate
Au-MSS	Gold core and mesoporous silica shell nanoparticle
BCL-2	B-cell lymphoma 2
BET	Brunauer–Emmett–Teller
BH3	BCL-2 Homology domain 3
BJH	Barrett–Joyner–Halenda
CD4 T	Cluster of differentiation 4-positive lymphocyte
CLSM	Confocal laser scanning microscopy
CT	Computer tomography
CTAB	Hexadecyltrimethylammonium Bromide
CTALA4 mAb	Cytotoxic T lymphocyte-associated antigen monoclonal antibody
CTL	Cytotoxic T lymphocyte
DIC	Differential Interference Contrast
DMEM-F12	Dulbecco's Modified Eagle Medium: nutrient mixture F-12
DMEM-HG	Dulbecco's Modified Eagle medium-high glucose
DMSO	Dimethyl sulfoxide
DNA	Deoxyribonucleic acid
Dox	Doxorubicin
ECM	Extracellular matrix
EGFR	Epidermal growth factor receptor
EPR	Enhanced permeability and retention
EtOH	Ethanol
FBS	Fetal bovine serum
FDA	Food and Drug Administration
FGF	Fibroblast growth factor
FibH	Primary normal human dermal fibroblast
FTIR	Fourier transform infrared spectroscopy
HeLa	Human negroid cervix epithelioid carcinoma
HGF/c-Met	Hepatocyte growth factor/hepatocyte growth factor receptor

K^-	Negative Control
K^+	Positive Control
LSPR	Localized surface plasmon resonance
MDSC	Myeloid-derived suppressor cell
MFI	Mean fluorescence intensity
MSC	Mesenchymal stem cell
MSS	Mesoporous silica shell
MTT	3-(4, 5-dimethylthiazolyl-2)-2,5-diphenyltetrazolium bromide
NIR	Near infrared
NK/T	Natural killer and natural killer T cell
NR	Nanorod
PARP	Poly ADP ribose polymerase
PBS	Phosphate-buffered saline
PDGF	Platelet-derived growth factor
PEG	Polyethylene glycol
Peoz	Polyoxazoline
PGA	Polyglycolic acid
P-gp	Glycoprotein-P
PNIPAAM	Poly(N-isopropylacrylamide)
PTT	Photothermal therapy
PVP	Poly(vinyl pyrrolidone)
RES	Reticuloendothelial system
ROS	Reactive oxygen species
s.d.	Standard deviation
TEM	Transmission electron microscopy
TEOS	Tetraethylorthosilicate
Th2	Helper type 2 lymphocyte
Treg	Regulatory T cell
UV-vis	Ultraviolet-visible
VEGF	Vascular endothelial growth factor
αSMA	Alpha smooth muscle actin

Chapter 1

Introduction

1. Introduction

1.1. Cancer

1.1.1. Cancer prevalence and statistics

Cancer is one of the leading causes of human death in the world. Only in 2012, it was estimated that fourteen million new cancer cases were diagnosed and eight million cancer deaths occurred worldwide (Torre *et al.*, 2015). In the current year, recent studies report above two million of new cancer cases and about of six hundred thousand cancer-related deaths occurred only in the United States of America (Siegel *et al.*, 2015). In Portugal, accordingly to the reports from *Direção Geral de Saúde* (2015), in 2020 almost fifty thousand new cases will be diagnosed. Further, this number has tendency to increase and it is expected that the new cancer cases will be superior to sixty-two thousand in the year of 2035 (Miranda *et al.*, 2015). Furthermore, depending on the gender, there are some types of cancers that have higher incidence and mortality rates. In men, the most common types are prostate, lung/bronchus and colorectal cancers, whereas for the women the breast, lung/bronchus and colorectal cancers arise as the most prevalent ones (Siegel *et al.*, 2015).

These alarming numbers of cancer incidence and mortality are exacerbated by the aging and growth of the global population (Torre *et al.*, 2015). Further, there are several risk factors such as hormones secretion, genetic predisposition, exposure to environmental (e.g. radiation and chemical compounds), infectious agents, and individual behaviors (e.g. tobacco, food and alcohol consumption) that may increase the probability to develop cancer (Jemal *et al.*, 2011).

1.1.2. Cancer development and hallmarks

Cancer development is a highly complex process that involves the interaction of different players (Joyce and Pollard, 2009, Quail and Joyce, 2013). This disease is characterized by the transformation of normal cells into cancer cells, involving the accumulation of several changes in the gene expression patterns (Floor *et al.*, 2012). Initially, the cancer was presented as a single mass of cancer cells displaying a continuous and uncontrolled proliferation that could invade and colonize the surrounding tissues or even other sites of the human body (Hanahan and Weinberg, 2000). However, the concept of cancer evolved and nowadays it is considered a much more complex tissue that is also comprised by the surrounding tumor microenvironment (Figure 1) (Joyce and Pollard, 2009).

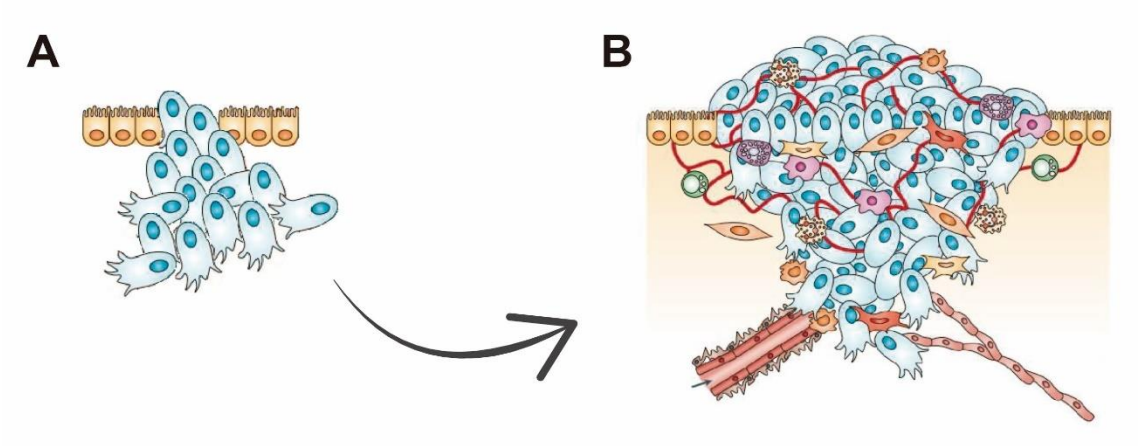

Figure 1 - Evolution of the cancer concept. (A) Reductionist view of the cancer, in which the tumor is only composed by cancer cells. (B) Current view of tumor microenvironment is composed by several types of cells, such as malignant cells, endothelial cells, pericytes, fibroblasts, immune system cells and extracellular matrix. The cross-talk between these elements contribute to cancer progression and maintenance (Adapted from (Joyce and Pollard, 2009)).

Presently, the tumor microenvironment is seen as being comprised of endothelial cells, pericytes, fibroblasts, some types of immune system cells, extracellular matrix (ECM) and other cells (Figure 2) (Pietras and Ostman, 2010, Hanahan and Coussens, 2012). The establishment of the cross-talk interactions between the cancer cells and the other elements of the tumor microenvironment can trigger pro-survival, proliferation and invasion pathways in cancer cells, which are of critical importance for the cancer establishment and development (Quail and Joyce, 2013). Additionally, these interactions between the tumor microenvironment elements allow the cancer cells to evolve, acquire and maintain certain key characteristics designated as "cancer hallmarks" (Hanahan and Weinberg, 2000, Hanahan and Weinberg, 2011).

One important characteristic of cancer cells is their capacity to maintain proliferative signaling, since they are able to produce their own growth signals and, thus become independent of normal stimulus provided by the surrounding tissues (Hanahan and Weinberg, 2000, Witsch *et al.*, 2010). Moreover, the cancer cells are capable of evading the anti-proliferative signals responsible for the maintenance of the tissue homeostasis. The tumor suppressors, such as retinoblastoma-associated proteins, operate as regulators and they determine if cell proliferates or enter into apoptosis. In cancer cells, this pathway is usually defective and the continuous cell proliferation is allowed (Hanahan and Weinberg, 2000, Hanahan and Weinberg, 2011).

Furthermore, these cells have the capacity to avoid the programmed cell death mechanisms (e.g. apoptosis) through the enhanced expression of anti-apoptotic proteins, such as those of B-cell lymphoma 2 (Bcl-2) family (Kelly and Strasser, 2011, Giampazolias and Tait, 2016). Moreover, the mutation of p53 tumor suppressor gene and the consequent loss of p53 protein function (apoptosis promoter) allows cancer cells proliferation (Hanahan and Weinberg, 2000).

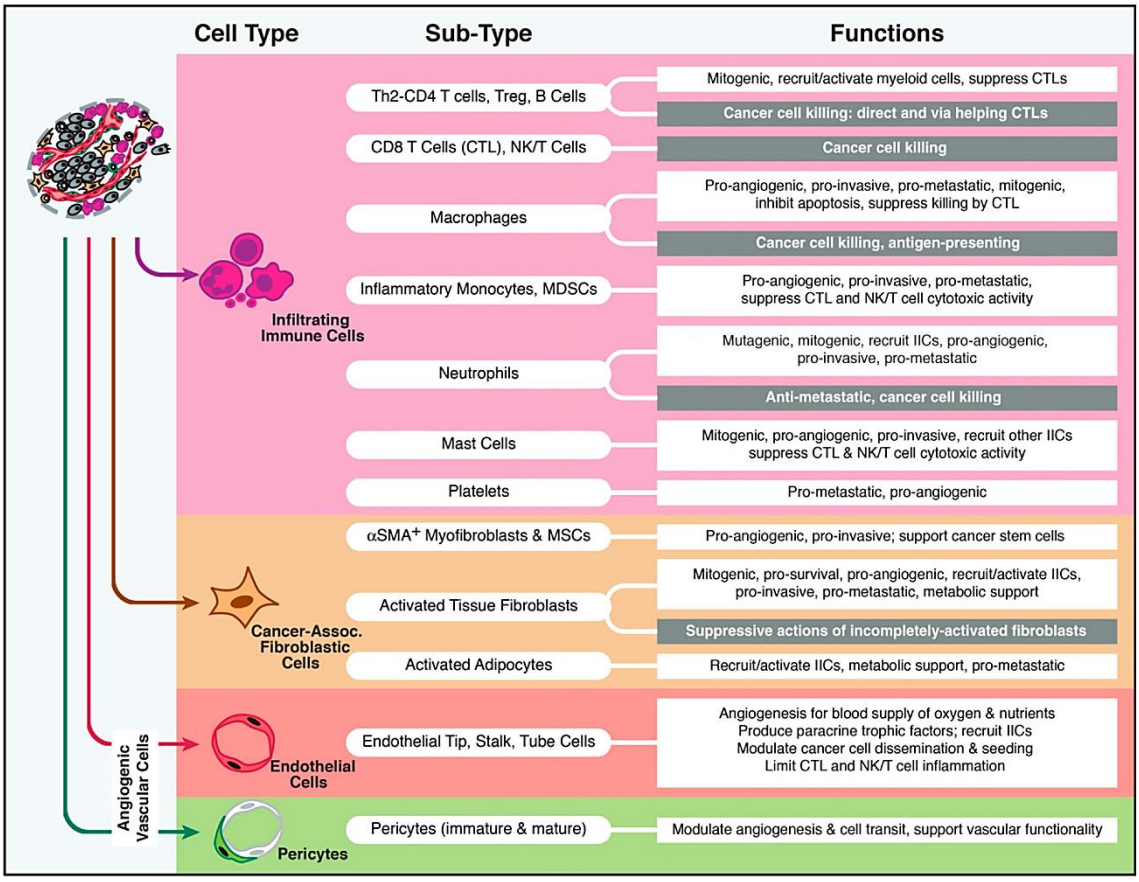

Figure 2 – Representation of the different cell types that are found on tumor microenvironment and their respective roles in cancer maintenance and progression. Helper type 2 lymphocyte (Th2), cluster of differentiation 4-positive lymphocyte (CD4 T), regulatory T cell (Treg), cytotoxic T lymphocyte (CTL), natural killer and natural killer T cell (NK/T), myeloid-derived suppressor cells (MDSCs), alpha smooth muscle actin (αSMA), mesenchymal stem cells (MSCs) (Adapted from (Hanahan and Coussens, 2012)).

Additionally, cancer cells have the capacity of unlimited replication. In normal cells, with the successive cycles of replication, the ability to conserve the chromosomal ends (telomeres) is impaired, which can lead to cell death due to deoxyribonucleic acid (DNA) damage (i.e. cell senescence). However, in cancer cells, through the overexpression of telomerase, the telomeric integrity of the DNA is maintained, which avoids the cell senescence or apoptosis (Artandi and DePinho, 2010, Hanahan and Weinberg, 2011). Moreover, the uninterrupted supply of oxygen and nutrients is pivotal for tumor growth and survival. In order to allow the correct nutrient supply/waste exchange equilibrium, the cancer cells are able to activate the angiogenic machinery, with the adjustment of the expression of angiogenesis inducers or inhibitors. For example, the vascular endothelial growth factor (VEGF), fibroblast growth factor (FGF), platelet-derived growth factors (PDGF) and angiopoietins are often found overexpressed in tumors and they contribute for stimulating the formation of new blood vessels (Hanahan and Weinberg, 2000, Goel and Mercurio, 2013). Another important hallmark that is found in cancer cells is their capacity to invade other tissues and initiate the metastasizing process due to the altered expression of several proteins that are involved in cell-to-cell adhesion processes. The integrin and cadherin families are transmembrane proteins that are responsible for cell-ECM

and cell-cell adhesion. In tumors, the E-cadherin protein is down-regulated, which can lead to the loss of cell-cell adhesion, thus facilitating the colonization of other tissues by the cancer cells (Hanahan and Weinberg, 2000, Pickup *et al.*, 2014).

Recently, additional cancer hallmarks have been proposed (Figure 3). The cancer cells also demonstrate the capacity to reprogram its metabolism in order to enhance the cancer cells proliferation and tumor progression. Further, the cancer cells have also the capacity to avoid the recognition by the immune system and their subsequent destruction (Hanahan and Weinberg, 2011). However, it is important to notice that before the cancer cells be able to acquire these important hallmarks there are essential pre-required factors, such as the cell genomic instability (i.e. allows gene expression variations) and an inflammatory state (i.e. the presence of inflammatory cells in tumor tissue leads to the release of mutagenic chemical compounds) that promote the acquisition of a malignancy phenotype by cancer cells (Hanahan and Weinberg, 2011).

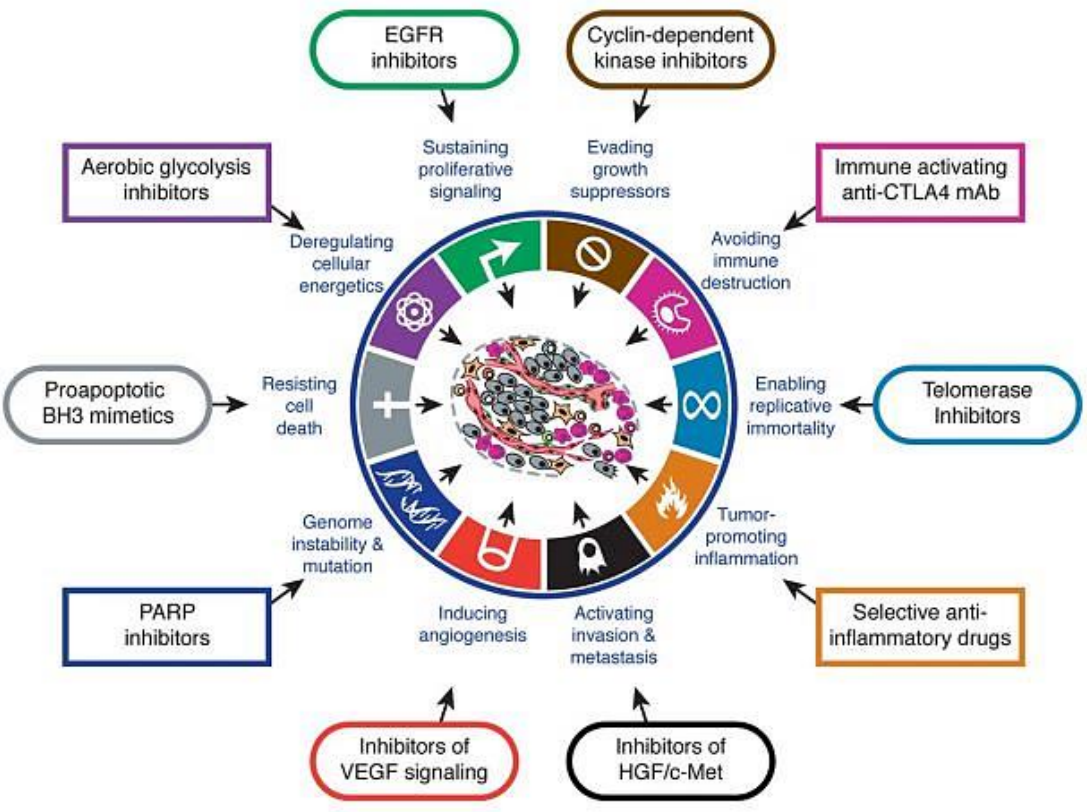

Figure 3 - Hallmarks of cancer and the respective possible therapeutic targets. Poly ADP ribose polymerase (PARP), Cytotoxic T-lymphocyte-associated antigen monoclonal antibody (CTLA4 mAb), epidermal growth factor receptor (EGFR), hepatocyte growth factor/hepatocyte growth factor receptor (HGF/c-Met), BCL-2 Homology domain 3 (BH3) (Adapted from (Hanahan and Weinberg, 2011).

1.1.3. Conventional therapies

The cancer treatments used in the clinic include chemotherapy, surgery, radiotherapy, hormone therapy and stem cell transplantation (DeSantis *et al.*, 2014). Moreover, these treatments can also be combined to increase their therapeutic effectiveness. In fact, the combination of surgery with radiotherapy or/and chemotherapy has been the most common method employed to fight cancer (DeSantis *et al.*, 2014).

The chemotherapy, the first-line treatment used for cancer therapy, uses highly cytotoxic agents such as anthracyclines and taxanes (Dong and Mumper, 2010). However, the administration of these compounds has several implications due to their low water solubility, rapid degradation, low selectivity and weak bioavailability (Holohan *et al.*, 2013, Hu *et al.*, 2016, Moreira *et al.*, 2016). Chemotherapeutics induce harsh side effects, which usually leads to the reduction of bone density, cardiotoxicity, fatigue, infertility, pain, pulmonary and sexual dysfunctions, that are a consequence of the administered dose and number of treatment procedures (Rebucci and Michiels, 2013, Siegel *et al.*, 2015, Moreira *et al.*, 2016).

Moreover, the cancer cells can also acquire multidrug resistance (MDR) phenotype, which further decreases the therapeutic effectiveness. The MDR mechanisms commonly observed in cancer cells involve an increased drug efflux (membrane transporters), drug target mutations, DNA damage repair, modulation of cell death mechanisms (apoptotic progression) and activation of alternative signaling pathways (Breier *et al.*, 2013, Holohan *et al.*, 2013, Rebucci and Michiels, 2013). Further, the acquisition of these MDR mechanisms in response to one cytotoxic therapeutic agent can also lead to the development of resistance to other chemotherapeutic agents, even those with unrelated structure (i.e. cross-resistance phenomenon) (Dong and Mumper, 2010, Holohan *et al.*, 2013).

The membrane transporters that act as drug efflux pumps are one of the most investigated MDR mechanisms. For example, the glycoprotein-P (P-gp) is a member of the ATP (adenosine triphosphate)-binding cassette (ABC) transporters family, a group of transmembrane proteins, that transport molecules to the exterior of the cell by the ATP hydrolysis. Generally, the P-gp is overexpressed on the membrane of cancer cells and their expression can also be further enhanced in response to the action of chemotherapeutics. The action of this efflux pump avoids the intracellular accumulation of anticancer drugs impairing the drug action and decreasing their therapeutic effect (Breier *et al.*, 2013, Hu *et al.*, 2016). The presented therapeutic limitations and the cancer specificities demand the development of new therapies.

1.2. Nanotechnology: Nanoparticles aimed for cancer therapies

The Nanotechnology is a multidisciplinary area that comprises the life sciences, material engineering and medicine, and provide novel solutions for improving not only the cancer therapy but also its diagnosis (Wang *et al.*, 2012a, Tong and Kohane, 2016). In cancer-related

applications, the inherent properties that these nano-sized platforms (1 to 1000 nm) present prompted their application in cancer therapy diagnosis, monitoring or in the theranostic applications (Xu *et al.*, 2015).

1.2.1. Nanoparticles benefits for cancer treatments

The application of nanotechnology in cancer therapy, in particular on chemotherapy, is aimed to overcome the limitations of free drug delivery and simultaneously enhance the treatment efficacy (Xu *et al.*, 2015, Kemp *et al.*, 2016).

Nanoparticles have the ability to improve the solubility and the chemical stability of poorly water-soluble anticancer drugs. Moreover, the nanoparticles are also capable of protecting the drugs during the circulation in the human body, which prevents their rapid degradation or excretion. Moreover, the nanoparticles can also avoid the premature interaction of therapeutic molecules with biological constituents, that can affect their pharmacokinetic profile and decrease their therapeutic potential (Wicki *et al.*, 2015).

Furthermore, nanoparticles can take advantage of the tumor tissue architecture, which displays an abnormal and leaky tumor vasculature and also an impaired lymphatic drainage, to be preferentially accumulated in tumor, the well-known enhanced permeability and retention (EPR) effect (see Figure 4 for further details) (Maeda, 2015). The blood vessels of tumors vasculature display fenestrae with 400 to 600 nm that allow nanoparticles escape from blood circulation into the tumor tissue. Moreover, due to the impaired lymphatic vasculature, the nanoparticles removal through the lymphatic drainage do not occur, thus favoring the nanoparticles accumulation in the tumor tissues. However, the dense ECM and high interstitial pressure present at the tumor site prevent the nanovehicle penetration into deeper regions of the tumors (Blanco *et al.*, 2015).

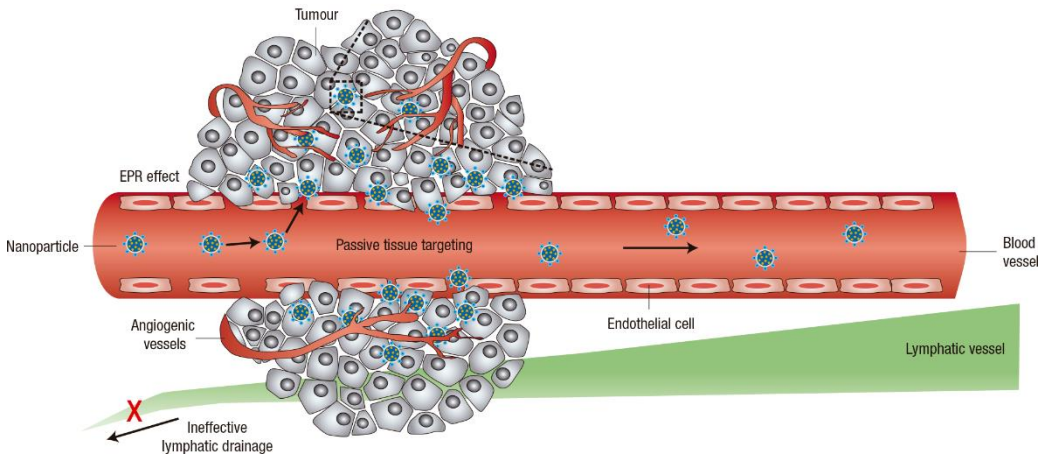

Figure 4 - Schematic representation of nanoparticles extravasation through the tumor vasculature, i.e. the EPR effect (Adapted from (Peer *et al.*, 2007)).

Further, the nanoparticles are also capable of carrying large amounts of drugs or even transport simultaneously two or more therapeutic agents (i.e. combinatorial therapy), in order to produce a synergic therapeutic effect (Kemp *et al.*, 2016). Another important characteristic of the nanoparticles is their potential to entrap the therapeutic agents within its structure and release them in response to specific stimuli that are present at the tumor site (Wicki *et al.*, 2015, Kemp *et al.*, 2016). Such behavior decreases the premature interaction of the therapeutic agents with the biological tissues and consequent side-effects. Additionally, the nanoparticles can also be engineered to take advantage of ligand-receptor, antigen–antibody and other forms of molecular recognition for enhancing its accumulation in one specific tissue or cells (Farokhzad and Langer, 2009). In these approaches, the targeting component present on the nanoparticle surface is chosen to bind specifically to unique molecules overexpressed on tumor cells and that are absent in normal cells. This targeted delivery of the therapeutic agents improves their specificity towards the therapeutic target and decreases the non-specific biodistribution.

These nanoparticle features can potentiate the therapeutic effect of the conventional therapies by promoting the drug accumulation in the tumor, while, simultaneously, decrease the systemic toxicity and side effects associated with these therapies. Therefore, a wide number of different nanoparticles have been developed for co-delivering multiple payloads, enhancing transport properties, improving biodistribution, increasing drug accumulation and for optimizing the drug release profiles (Farokhzad and Langer, 2009, Wicki *et al.*, 2015).

1.2.2. Classes of nanocarriers

The controlled drug delivery mediated by nanoparticles has progressed over the years, as well as the nanoparticle requirements to be applied in the clinic. The first generation of drug delivery systems was produced by using simple materials and with the objective to promote a sustained drug release along time (i.e. the drug was released by dissolution, diffusion, osmose or ionic trades). Subsequently, the second generation of the nanocarriers was aimed to perform a stimuli-sensitive drug delivery, as well as to promote a preferential accumulation of the drug in the tumor tissue. The third and fourth (current) generations are based on the production of drug delivery systems with smart materials that are able to perform long term delivery (i.e. over six months), fast response kinetics to *in vivo* stimulus and that are able to surpass the biological barriers, in order to perform drug delivery (e.g. blood-brain barrier) (Albanese *et al.*, 2012). Furthermore, these systems besides allowing drug delivery, can also be used in imaging and diagnostic, or even act as photothermal mediators, biosensors and others (Huang *et al.*, 2011, Pekkanen *et al.*, 2014, Rocha-Santos, 2014).

Nowadays, nanoparticles are classified into two major classes taking into account the raw material used for their synthesis, organic or inorganic particles (Figure 5) (Jia *et al.*, 2013a, Sagnella *et al.*, 2014, Wicki *et al.*, 2015). Within the organic nanostructures, there are two

main classes, lipid-based and polymer-based nanoparticles. The lipid-based nanoparticles are usually formed as liposomes or lipidic micelles. The liposomes are composed by one or more phospholipid bilayers, that display a spherical organization and an aqueous core. This liposomal organization allows the transport of both water soluble drugs (in the aqueous core) as well as the hydrophobic ones (within the phospholipid bilayer). The Doxil® was the first liposome approved by Food and Drug Administration (FDA), in 1995, for cancer therapy. This liposomal nanocarrier loaded with Dox was coated with polyethylene glycol (PEG) to improve its blood circulation time in the human body (Wicki *et al.*, 2015). Lipidic micelles are generally composed by a monolayer of phospholipids organized in a micellar structure. This type of nanoparticles is particularly valuable for the encapsulation of hydrophobic molecules, which are entrapped in their hydrophobic core. However, lipid-based systems display some disadvantages that hinder their *in vivo* application, like limited stability, opsonization and low capacity to control the drug release (Akbarzadeh *et al.*, 2013).

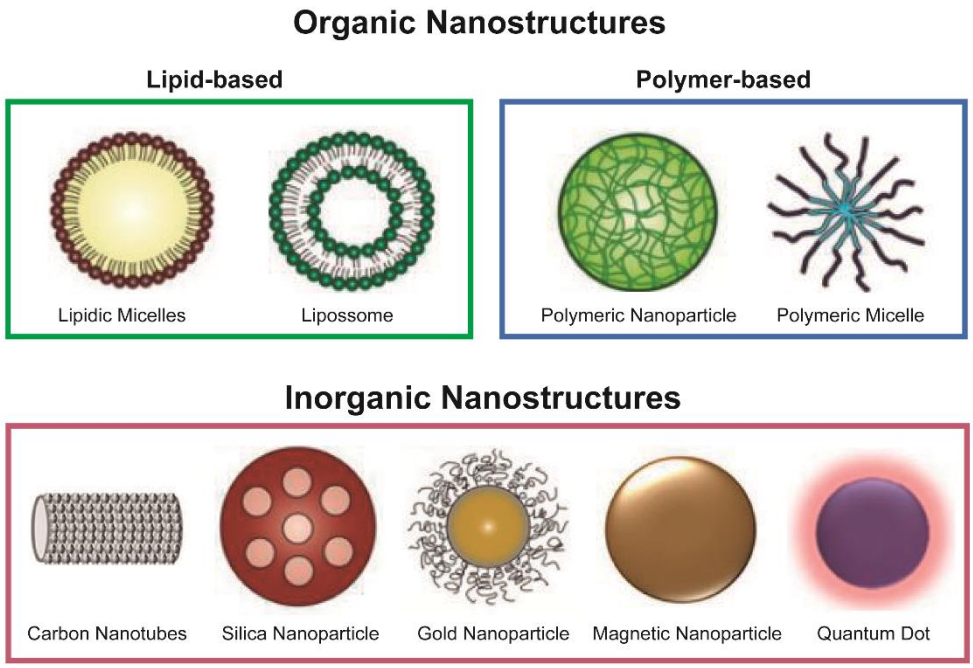

Figure 5 - Representation of the organic and inorganic based nanovehicles (Adapted from (Jia *et al.*, 2013a, Sagnella *et al.*, 2014, Wicki *et al.*, 2015)).

Among the polymer-based nanoparticles, polymeric micelles arise as one of the most used structures. They are prepared using amphiphilic polymers and their organization allows the encapsulation of poorly water-soluble drugs on the micelle core, which is formed by the hydrophobic segment of the polymer. The polymer hydrophilic shell is exposed to the solvent and it prevents the adsorption of plasma proteins and it increases nanoparticle blood circulation time (Elsabahy and Wooley, 2012, Wicki *et al.*, 2015). Nanoplatin® is a micellar structure composed of a copolymer (PEG-polyglycolic acid (PGA)) and it was conceived for Cisplatin delivery, being currently in phase 3 of clinical trials. This system demonstrated a

pharmacokinetic profile more advantageous than that displayed by free Cisplatin, leading to a reduction of cisplatin-related toxicity (Plummer *et al.*, 2011). Polymeric nanoparticles are usually produced by using hydrophobic polymers functionalized at their surface with hydrophilic polymers. The chemotherapeutics can be entrapped between the polymer chains or at the particle's surface in order to allow the encapsulation and transport of a wide range of therapeutics including drugs, proteins and nucleic acids. However, the polymeric-based nanoparticles have some disadvantages, such as their weak physicochemical stability that can induce changes in the morphology of the carriers (i.e. assembly and disassembly of nanoparticles during storage or blood circulation), which will affect the bioavailability of the loaded compounds. Further, the particle disassembly can also promote a premature release of the loaded cargo, which results in a decrease of therapeutic potential (Elsabahy and Wooley, 2012, Wicki *et al.*, 2015).

Inorganic nanostructures comprise quantum dots, magnetic nanoparticles, carbon nanotubes, silica nanoparticles and gold nanostructures (Figure 5) (Jia *et al.*, 2013a, Wicki *et al.*, 2015). Quantum dots are semiconductor nanocrystals, with a size up to 10 nm. They are mostly applied for bio-imaging, due to their broad absorption and emission peaks in the visible (400 - 700 nm) and near-infrared (NIR) region (700 – 1100 nm) (Nazir *et al.*, 2014). However, the hydrophobic surface of quantum dots requires their functionalization with biocompatible materials before their use in biological applications.

Magnetic nanoparticles such as superparamagnetic iron oxide nanoparticles can serve as contrast agents for imaging purposes. Moreover, these particles also have the capacity to generate heat in response to a magnetic field, allowing their application in magnetic hyperthermia. NanoTherm® is an example of the commercial available inorganic nanoparticles used for cancer therapy. These nanoparticles demonstrated to be effective in the treatment of glioblastoma (Maier-Hauff *et al.*, 2011, Wicki *et al.*, 2015). However, the possible long-term toxicity of this type of nanoparticles is not yet fully characterized.

Carbon nanotubes are multifunctional platforms that can be used for imaging, drug delivery and thermal ablation of cancer (Madani *et al.*, 2011). The hydrophobic character of this type of carrier also requires their functionalization with hydrophilic molecules to improve their stability and biocompatibility. Additionality, the *in vivo* long-term toxicity of these materials is still a matter of debate (Kumari *et al.*, 2016).

Silica nanoparticles, namely those with a mesoporous structure, can be used to deliver both hydrophilic and hydrophobic molecules. These type of nanoparticles have a high stability and are biocompatible (Moreira *et al.*, 2016). On the other hand, gold-based nanoparticles can be used for imaging and thermal ablation of tumors. However, gold structures have some toxicity, which requires their further functionalization (Akhter *et al.*, 2012). Similar to the other inorganic systems, the main drawbacks associated with silica- and gold-based nanoparticles are

associated with their non-biodegradable profile. These materials are discussed in more detail in section 1.3.

So far, there are no inorganic-based nanoparticles approved by FDA to be used in the clinic. However, there are several undergoing clinical trials for cancer therapy or imaging where gold and/or silica-based nanoparticles are currently being assayed (Wicki *et al.*, 2015).

1.2.3. Nanoparticles biodistribution and design

Nanovehicles administration in the human body can occur by different routes, such as oral, nasal, vaginal, transdermal, pulmonary, intramuscular and intravenous, being the latter the most commonly used (Mitragotri *et al.*, 2014, Park, 2014).

The application of nanoparticles in a biological environment involves different phases and the contact with several body components (Petros and DeSimone, 2010, Albanese *et al.*, 2012, Ernsting *et al.*, 2013). Considering an intravenous administration, the first phase of the nanoparticle journey is the systemic circulation (Figure 6). Once inside the blood stream nanoparticles must remain stable, in order to avoid their aggregation or degradation (e.g. oxidation or hydrolysis) (Mitragotri *et al.*, 2014). During their circulation in the blood stream, nanoparticles have to evade the clearance by renal filtration and the uptake by the reticuloendothelial system (RES) organs, namely liver and spleen, that can entrap and degrade nanoparticles (Ernsting *et al.*, 2013). Moreover, during systemic circulation, nanoparticles must avoid the adsorption of plasma proteins (serum albumin, complement components and immunoglobulins) to their surface. The adsorbed proteins will be recognized by phagocytic cells, leading to nanoparticles clearance (Blanco *et al.*, 2015, Hoshyar *et al.*, 2016).

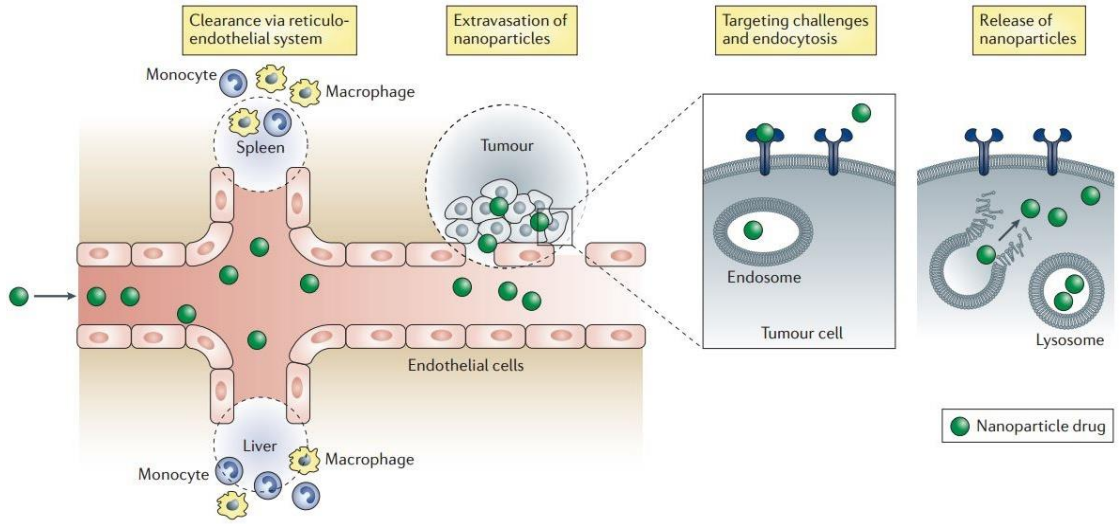

Figure 6 - Main barriers found by nanoparticles during their circulation in the blood. The nanoparticles must be able to avoid renal, liver and spleen clearance to increase their half-time in blood circulation. At the target site, particles have to extravasate through the leaky tumor vasculature and ultimately interact with the target cells to exert its therapeutic effect (Adapted from (Mitragotri *et al.*, 2014)).

After avoiding the possible barriers encountered during systemic circulation, nanovehicles must be able to reach the tumor zone and extravasate from the tumor vessels into the tumor tissue. Moreover, nanoparticle must also extravasate and penetrate in tumor tissue in a high concentration, that assures a therapeutic effect. Nanoparticles extravasation is largely influenced by abnormal and leaky tumor vasculature and also by impaired lymphatic drainage (EPR effect) (Maeda, 2015). Subsequently, in order for nanoparticles to reach the tumor cells, they must penetrate through the tumor mass. This process is impaired by the ECM and by the high interstitial fluid pressure that is found in tumors, thus preventing the penetration of nanovehicles into deeper regions of the tumor and, also causing a heterogeneous nanoparticle distribution (Blanco *et al.*, 2015). Lastly, the nanosystems should be internalized by cancer cells and release their content in the intracellular compartment (Ernsting *et al.*, 2013).

The successful fulfillment of these phases is influenced by several nanoparticles parameters, namely their size, charge, surface composition and shape (Figure 7) (Petros and DeSimone, 2010, Albanese *et al.*, 2012).

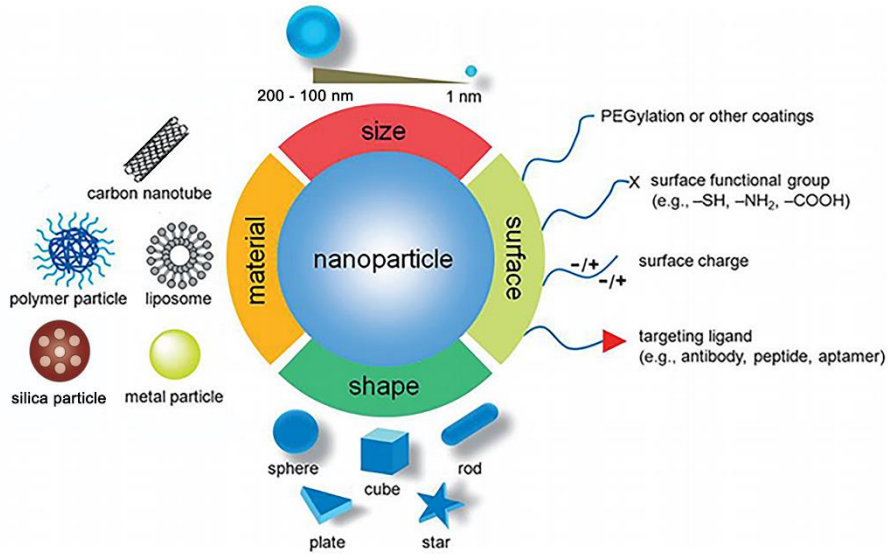

Figure 7 - Physicochemical properties displayed by nanoparticles that influence their behavior in biological environments (adapted from (Sun *et al.*, 2014, Wicki *et al.*, 2015)).

2.2.3.1. Nanoparticles size

There are various *'size thresholds'* that should be taken into account during the nanoparticle design (Figure 8). Particles with a size lower than 5 nm are rapidly eliminated by renal filtration. Moreover, the size also regulates the nanoparticles filtration and uptake by RES organs. Nanoparticle with sizes lower than 50 nm can interact with hepatocytes since these nanoparticles can extravasate through the liver fenestrations (50 – 100 nm). On the other side, nanoparticles larger than 200 nm accumulate in the spleen, since these may not extravasate through splenic slits (200 – 500 nm). Moreover, larger nanoparticles are also sequestered by the macrophages residing in liver (Kupffer cells) and spleen (Arami *et al.*, 2015). Considering these

size limits and those imposed by the EPR effect, the ideal nanoparticle size is considered to be comprehended between 50 and 200 nm (Hoshyar *et al.*, 2016).

Nanoparticles size also influences their tumor penetration. In general, bigger nanoparticles have a low tumor penetration capacity, whereas the smaller ones are more prone to penetrate deeper and faster in the tumor mass (Ernsting *et al.*, 2013, Hoshyar *et al.*, 2016). Finally, nanoparticles cellular internalization is also affected by their size. Small nanoparticles (4-10 nm) can become internalized in cancer cells by direct transposition of the lipid bilayer membrane (Mao *et al.*, 2013).

On the other hand, bigger nanoparticles are internalized by pinocytosis, in a process comprising clathrin-dependent endocytosis (~120 nm, destined to lysosomes) or clathrin-independent endocytosis. The latter pathway encompasses the caveolin-dependent endocytosis (~60 nm), clathrin- and caveolin-independent endocytosis (~120 nm) and micropinocytosis (> 1 μm) (Sahay *et al.*, 2010, Yameen *et al.*, 2014). In this way, size affects the fate of internalized nanoparticles since some uptake routes direct the nanoparticles to the lysosomes, which can lead to the degradation of the loaded cargo by hydrolytic mechanisms (Ernsting *et al.*, 2013).

2.2.3.2. Nanoparticles charge

Nanoparticles charge is an important parameter that affects the particle circulation time in the bloodstream (Figure 8). Nanoparticles that are highly positive (zeta potential > +10 mV) will interact with blood proteins, leading to their opsonization and clearance. The negatively charged nanovehicles (zeta potential < -10 mV) will be uptaken by RES. Thereby, a neutral charge (±10 mV) is considered ideal for nanoparticles being less prone to suffer opsonization and RES uptake (Ernsting *et al.*, 2013).

Additionality, nanoparticles charge may impair their tumor penetration by interacting with the charged components of the tumor ECM. Positively charged particles tend to interact with hyaluronic acid, while those with a negatively charged surface interact with collagen. Thus, neutrally charged nanoparticles are also the most appropriated for penetrating into the tumor mass (Ernsting *et al.*, 2013, Blanco *et al.*, 2015).

2.2.3.3. Nanoparticles surface composition

The components that form the nanoparticles surface are important players on nanovehicles biodistribution (Figure 8). Nanoparticles surface can be functionalized with hydrophilic polymers in order to improve their solubility and stability. The most commonly adopted polymer to achieve such properties is PEG. PEG coatings can also reduce nanoparticles opsonization, protect them from degradation and reduce their uptake by macrophages (Petros and DeSimone, 2010, Ernsting *et al.*, 2013).

However, the properties conferred by this type of coating depend on some factors, such as PEG density and molecular weight. Recently, some research groups have demonstrated that anti-PEG antibodies are produced after injection of PEGylated nanomaterials, which leads to the rapid elimination of nanoparticles in the subsequent administrations – a phenomenon termed Accelerated Blood Clearance. Due to that, other types of coatings are being investigated , such as Polyoxazolines (Peoz) and Poly(glycerol) (Amoozgar and Yeo, 2012, Lila *et al.*, 2013).

Nanomaterials surface can also be coated with inorganic materials, such as silica. These inorganic materials can increase the nanoparticles solubility, protect their internal structure from degradation and confer thermal and chemical stability. The inorganic materials can also be easily functionalized, which can further improve their potential for application in the clinic (Liu *et al.*, 2015b). Moreover, nanoparticles surface can also be grafted with targeting ligands, e.g., transferrin, folic acid and antibodies, in order to improve their selectivity towards cancer cells (Ernsting *et al.*, 2013, Bertrand *et al.*, 2014).

2.2.3.4. Nanoparticles shape

The shape is also an important parameter that will affect the nanoparticles interaction with the human body. During blood circulation, the nanoparticle shape will affect their interaction with the macrophages and consequently impact on the nanoparticle circulation time. For instance, worm-like and rod-shaped nanocarriers are less phagocytized than the spherical-shaped ones (Champion and Mitragotri, 2009, Janát-Amsbury *et al.*, 2011).

Furthermore, the shape also affects the capacity of nanomaterials to reach the tumor zone. In this topic, there is some controversy in the literature. Janát-Amsbury *et al.* verified that PEGylated gold nanorods (NRs) achieve a higher tumor accumulation than gold nanospheres, most likely due to their longer blood circulation time and lower uptake by the liver and spleen (Janát-Amsbury *et al.*, 2011). In another work, Black and co-workers reported that PEGylated gold nanospheres presented the highest tumor accumulation, followed by nanocages, nanodisks and NRs. In this report, the spherical nanoparticles also displayed a higher blood circulation time and a lower RES organ uptake than the other structures, leading to their higher tumor accumulation (Black *et al.*, 2014). Moreover, it was also observed that elongate-shaped materials are more difficult to remove from the tumor site than those spherically shaped (Ernsting *et al.*, 2013, Hoshyar *et al.*, 2016). In addition, the nanoparticles shape also affects the particles penetration and distribution within the tumor tissue. Black and colleagues observed that gold NRs and nanocages presented a wider tumor distribution, whereas the nanospheres and nanodisks were mainly confined to the tumor periphery (Black *et al.*, 2014).

Moreover, the effect of the nanoparticle shape on the cellular uptake appear to be material dependent, i.e., silica and iron oxide non-spherical nanocarriers present an enhanced cellular internalization, while for polymers and gold, the spherical shaped particles are the ones that present the better cellular internalization (Ernsting *et al.*, 2013).

The contribution of nanoparticles shape on the different processes above described has not yet fully characterized and it is also a subject of strong debate since the data available in the literature is often contradictory. Therefore, the fundamental research in this topic is strongly encouraged.

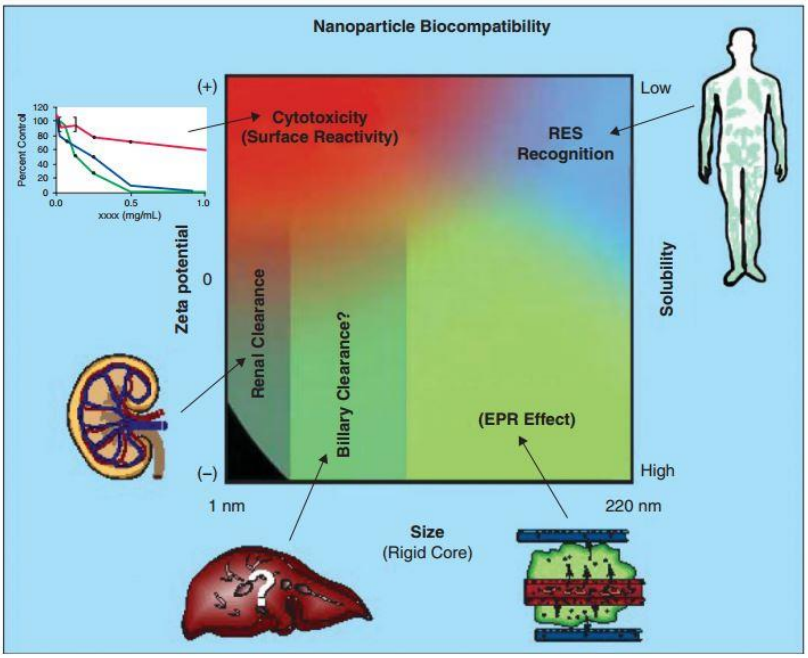

Figure 8 - Representation of physicochemical characteristics of nanoparticles that influence their biological performance. The correlation between the particle design, such as size, zeta potential (represented as surface charge) and solubility with the particle biocompatibility, route of uptake and clearance (shown in green), cytotoxicity (red), and RES recognition (blue) is presented in this scheme (Adapted from (McNeil, 2009)).

1.3. Gold nanoparticles

In recent years, inorganic nanoparticles have received a huge attention owing to their unique physicochemical properties. The inorganic nanoparticles inertness, stability, optical and magnetic properties (properties that are difficult to observe in organic particles) makes them an interesting approach for biomedical applications (Huang *et al.*, 2011).

1.3.1. Methods used for gold nanoparticles synthesis

Gold nanoparticles can be synthesized by two different approaches, namely *top-down* and *bottom up*. As the name suggests, the *top-down* starts from gold in a bulk state that is broken down to create gold nanoparticles with the desired dimensions, resorting to a specific pattern or matrix (Zhao *et al.*, 2013). The *bottom-up* approach is based on chemical (chemical reduction) or biological (use of plants or micro-organisms) methods to produce gold nanoparticles (Ahmed *et al.*, 2016). The *bottom-up* approach is usually divided into two phases, the nucleation and growth, when these two stages occur simultaneously in the same procedure the synthesis is denominated by *in situ* method, while in another way, the process is called seed-growth method (Zhao *et al.*, 2013).

The normal oxidation stages of gold are +1 (aurous compound or Au [I]) and +3 (auric compound or Au [III]). Usually, all synthesis methods involve the reduction of Au [III] derivatives, such as chloroauric acid, to Au (0) or Au atoms (non-oxidized state), which act as the center of nucleation for other reduced gold ions (Jain *et al.*, 2012).

So far, several methods have been used for the synthesis of gold nanoparticles, for allowing the production of nanoparticles with different sizes and shapes. The *in situ* Turkevich method, later improved by Frens, was the first technique used to produce gold nanoparticles (Turkevich *et al.*, 1951, Frens, 1973). The main principle in this approach is the reduction of chloroauric acid by trisodium citrate, which also acts as stabilizing capping agent by electrostatic interactions. Depending on the gold source and on the trisodium citrate ratio it is possible to produce spherical gold particles with sizes between 15 and 100 nm. When a great amount of citrate salt is used, small and stable gold nanoparticles are formed. On the other side, a low concentration of trisodium citrate leads to bigger and aggregated particles. However, the synthesis is considered unreliable for particles larger than 35 nm and the trisodium citrate is not capable of stabilizing the particles when they circulate in the blood stream (Turkevich *et al.*, 1951, Frens, 1973, Jain *et al.*, 2012, Nicol *et al.*, 2015). Moreover, other commonly used *in situ* method is the Brust-Schiffrin method. This technique involves the use of two solvent phases (i.e. water and toluene) and the addition of the desired amount of a thiolate-compound. With this approach, it is possible to obtain thiolate-stabilized gold nanoparticles that possess less than 5 nm of size. Herein, the sodium borohydride is used as a reducing agent, since it has a stronger redox potential than trisodium citrate, the produced nanoparticles are smaller (< 5 nm) than those obtained by Turhevich method (10 – 15 nm). Unlike Turhevich method, these nanoparticles need an additional capping agent to confer them a higher stability (such as benzyldimethyltetradecylammonium chloride) (Jain *et al.*, 2012, Perala and Kumar, 2013, Zhao *et al.*, 2013).

On the other hand, the seed-growth approach allows the formation of particles in a step-by-step method, thereby achieving an easier control over the particle size and shape (Zhao *et al.*, 2013). In general, two main steps are required for particle production. In the first stage, occurs the formation of a gold seed solution (small-size particles) by nucleation. Then, this solution is added to a solution denominated of “growth solution”, which is composed of a gold salt (e.g. chloroauric acid), stabilizing and reduction agents. Herein, the new reduced compound grows on the surface of the seed particles. This second step is more slow and can be repeated in order to modulate nanoparticles’ size (Alkilany *et al.*, 2013, Zhao *et al.*, 2013). The final shape and size are controlled by the amount of reducing agent and stabilizer (e.g. surfactants such as cetyltrimethylammonium bromide - CTAB) and their ratio to the gold precursor. The pH, temperature and growth time are also factors that influence the final shape and size of gold particles (Zhao *et al.*, 2013, Bao *et al.*, 2014). Therefore, anisotropic structures (i.e. non-

spherical) with different shapes, such as NRs, nanocubes and nanostars can be prepared by using the seed-growth approach (Alkilany *et al.*, 2013).

1.3.2. Gold nanoparticles properties and their applications in cancer

Gold nanoparticles possess unique properties that make them promising platforms for application in the biomedical field. In general, the tunable surface chemistry, morphology and physicochemical properties of gold nanostructures make them ideal for cancer therapy and also for diagnosis applications.

The surface chemistry of gold nanostructures is non-reactive and almost bio-inert, which allow them to be good candidates for both *in vitro* and *in vivo* applications (Cobley *et al.*, 2011). The easily tuning of the surface chemistry, namely through the formation of stable gold–thiolate bonds with molecules presenting thiol (–SH) or disulfide (S–S) groups, allows their conjugation with a wide variety of functional moieties (Cobley *et al.*, 2011, Dreaden *et al.*, 2012).

Furthermore, due to the high density of the gold, they can be used as contrast agents to enhance the contrast between tissues, that have similar or low x-ray attenuation, without increasing the dose of radiation that is administrated to the patient (Xi *et al.*, 2012, Cole *et al.*, 2015). In this way, gold nanoparticles can be used as contrast agents in computer tomography (CT), since they have a high x-ray absorption coefficient. For example, the absorption coefficients of gold and iodine (i.e. the most common contrast agent) when exposed to a x-ray beam with 100 keV are 5.16 and 1.94, respectively (Xi *et al.*, 2012). Moreover, due to the high molecular weight, gold nanoparticles display a longer vascular retention time (i.e. when compared to common contrast agents) that allow the acquisition of images for longer periods (Cole *et al.*, 2015). Furthermore, these particles can take advantage of the tumor tissue architecture, namely of the EPR effect, or be functionalized with target molecules in order to provide a selective and sensitive detection of possible metastasis by using CT images (Reuveni *et al.*, 2011).

Moreover, another important feature of gold nanostructures is their exceptional optical properties, since when these structures are exposed to electromagnetic radiation with specific wavelengths, a collective oscillation of electrons in resonance with the incoming light frequency occurs (Cobley *et al.*, 2011, Versiani *et al.*, 2016). The absorption of electromagnetic radiation energy can lead to the heat generation by the collective oscillation of electrons (Huang and El-Sayed, 2010, Cobley *et al.*, 2011). These electrons oscillations are also known as localized surface plasmon resonance (LSPR). The LSPR response of gold nanostructures can be influenced by size, shape and morphology of the nanoparticle, which results in strong absorption bands at certain wavelengths of the electromagnetic spectrum (Akhter *et al.*, 2012).

The typical spherical gold-based nanoparticles possess an absorption peak from 500 to 550 nm and with the increasing particle size a red shifting occurs (for values rightmost in the spectrum,

i.e., higher wavelengths) (Figure 9A). For example, gold nanoparticles with a size of 20 and 80 nm display different absorption peaks, namely at 520 and 550 nm (Alex and Tiwari, 2015).

In anisotropic structures, especially rod-shaped nanoparticles, the electron oscillations exist in two directions/orientations (short and long axis of the structure), creating two distinct bands in the spectrum with different intensities. The band resulting from oscillation along the short axis is similar to the one observed in gold nanospheres (it can be observed between the 500 to 550 nm). On the other hand, the oscillation along the long axis induces a stronger absorption band, called longitudinal band (Figure 9B) in the NIR region (700 to 1100 nm) of the electromagnetic spectrum (Cobley *et al.*, 2011, Alex and Tiwari, 2015). Through the control of the aspect ratio (length/width) of gold NR, it is possible to tune the longitudinal absorption band to a specific value (Huang *et al.*, 2008).

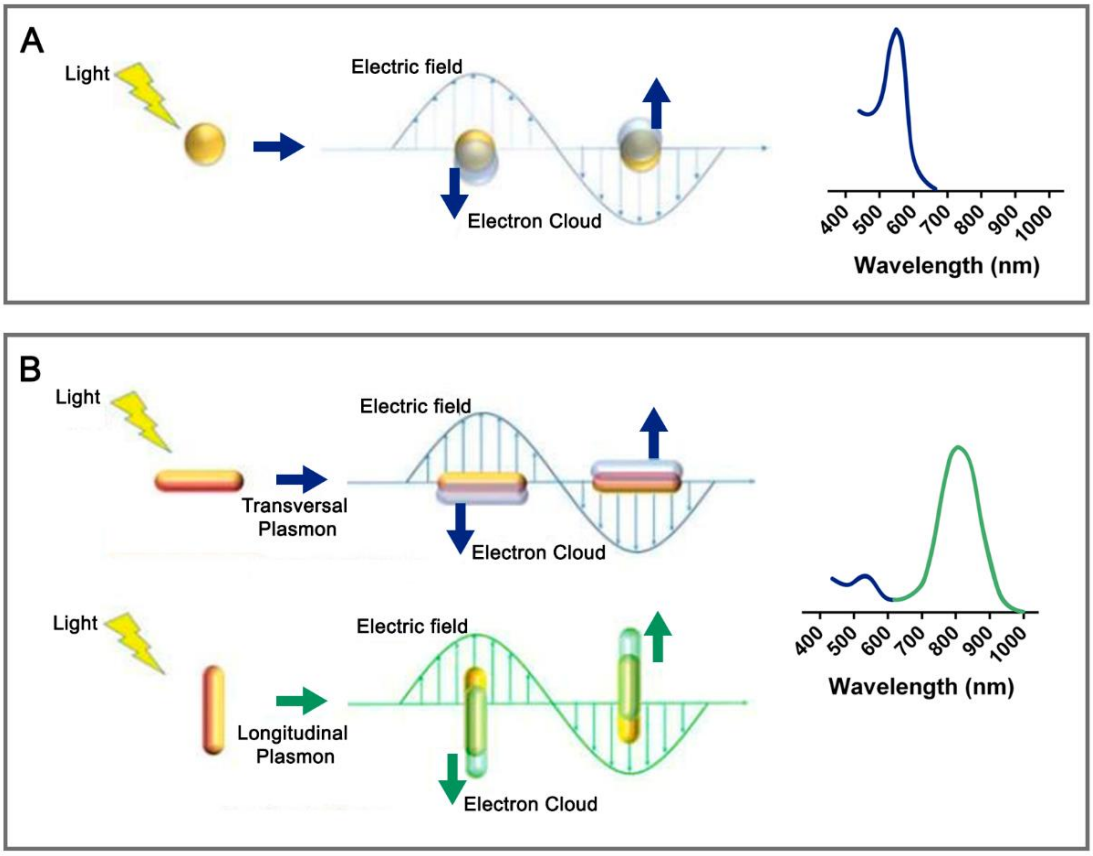

Figure 9 - Schematic representation of LSPR of gold nanoparticle through the coherent oscillation of electrons across the surface of the nanoparticle and the correspondent LSPR bands. (A) Spherical-shaped gold nanoparticle that displays one LSPR band. (B) Rod-shaped gold nanoparticle that displays two LSPR bands, namely a strong longitudinal band (green) and weak transverse band (blue) (Adapted from (Alex and Tiwari, 2015)).

The increase of the gold NRs aspect ratio is accompanied by an increase in the distance between two plasmon resonance bands, resulting in a shift of the longitudinal peak from the visible to the NIR region (Abadeer and Murphy, 2016). For instance, an aspect ratio of 3.1 corresponds to

a longitudinal absorption band at 700 nm, while gold NR with an aspect ratio of 4.8 display a peak around the 880 nm (Huang *et al.*, 2006).

Some gold-based nanoparticles have been applied for cancer photothermal therapy (PTT). In this therapeutic approach, nanoparticles are irradiated with light, and convert the absorbed radiation into heat, which can cause cellular damage (Wang *et al.*, 2013, Zou *et al.*, 2016). The exposition of cells to temperatures between 41 – 45 ˚C can impair DNA repair mechanisms, promote alterations in cellular metabolism, increase the production of reactive oxygen species (ROS) and sensitize cancer cells to therapeutic agents. Moreover, treatments at 50 ˚C can produce immediate cell death (necrosis) by promoting cell membrane collapse, protein denaturation, and mitochondrial and enzymatic dysfunctions (Chatterjee *et al.*, 2011, Chu and Dupuy, 2014).

In cancer PTT the utilization of NIR light is imperative (Abadeer and Murphy, 2016), due to the fact that major components of the body (water, hemoglobin, proteins and melanin) have minimal or none absorption in the 700–1100 wavelength range. In this way, the utilization of NIR light avoids the undesired interactions between the radiation and biological components as well as a good penetration depth. Such is fundamental to avoid non-specific heating on healthy tissues and guarantees that the radiation reaches the nanoparticles accumulated in tumors (Vogel and Venugopalan, 2003, Versiani *et al.*, 2016). For these reasons, the NIR absorption displayed by gold NRs has instigated their use in cancer PTT (Wang *et al.*, 2012b).

1.3.3. Limitations of gold nanostructures

Despite the wide scope of applications of gold nanostructures, there are some issues and limitations that impair their application in cancer therapy and diagnosis. The utilization of a cationic surfactant, such as CTAB, in the synthesis of gold-based nanosystems is crucial in the seed-growth method to develop particles with tunable shapes and sizes. However, CTAB has a negative impact on the nanoparticles biocompatibility, due to its toxicity, and impairs gold nanoparticles application in biological environments (Dreaden *et al.*, 2012, Bao *et al.*, 2014).

Another limitation of gold nanoparticles is their instability and propensity to aggregate when in contact with biological fluids (Dreaden *et al.*, 2012). Such phenomenon can produce alterations in nanoparticles size and have a negative impact on their bioavailability (Gupta *et al.*, 2016). In addition, gold-based nanomaterials structure and chemical features do not allow their application for drug delivery without post-synthesis modifications (Sasidharan and Monteiro-Riviere, 2015). Furthermore, gold nanostructures can suffer photodegradation. When bare gold nanoparticles are exposed to light for photothermal purposes, their physical integrity can be compromised and as a consequence, their photothermal heating capacity decreases (Chen *et al.*, 2010, Jalani and Cerruti, 2015). Thus, post-synthesis modifications of gold-based nanoparticles can be a promising approach for surpassing these limitations and potentiate gold-based nanosystems application in cancer therapy.

1.3.4. Coating or functionalization approaches used to improve gold nanostructures properties

The modification of gold nanomaterials surface is necessary to improve their optical properties, thermostability or to potentiate their therapeutic outcome.

Thiols have a natural affinity for gold nanoparticles surface and the covalent bond of thiolated molecules to gold nanoparticles' surface (*via* Au-S bond) has been widely described in literature (Gao *et al.*, 2012). However, the stability of thiol-gold chemical linkages can be impaired by reductive environments or by exchange with other thiolated molecules (Woehrle *et al.*, 2005, Ruff *et al.*, 2016).

Alternatively, gold nanoparticles surface can also be functionalized by passivation, using amphiphilic molecules (Heo *et al.*, 2015). The poly(vinyl pyrrolidone) (PVP) coating of gold nanostructures is an example of this strategy, and it is usually employed for improving the particles biocompatibility. The PVP binds to the surface of the gold nanoparticles through their hydrophobic polycarbonated chain. In this way, the PVP coating can also improve the stability of gold nanoparticles (Dhumale *et al.*, 2012). However, the application of PVP coatings in gold NRs did not protect their physical integrity under laser irradiation, leading to loss of the NIR absorption peak, which may hinder their potential application in PTT (Wang *et al.*, 2013).

Furthermore, PEG is one of the most commonly applied molecules to coat gold nanoparticles (Muddineti *et al.*, 2015). Functionalization of gold nanoparticles with PEG, a hydrophilic and biocompatible polymer, prevents their aggregation and avoids the adsorption of serum proteins on their surface (Niidome *et al.*, 2006). Gold nanostructures are usually PEGylated using thiol-terminated PEG (Ding *et al.*, 2013). However, a recent study described that gold nanospheres and NRs stabilized with PEG-SH suffer alterations in their stability over time. Ruff and collaborators observed that nanoparticles aggregated when incubated in saline solution or in the culture medium, which was attributed to the possible loss of PEG-SH coating (Ruff *et al.*, 2016).

Moreover, electrostatic interactions established between negatively charged molecules and the positively charged surface of gold nanoparticles can be explored to functionalize these materials (Versiani *et al.*, 2016). The main drawback of this type of functionalization is correlated with its easy disruption, which becomes more evident with variations in the pH and ionic composition of the medium where the nanoparticles are dispersed.

1.3.4.1. Silica Coating

Gold-based nanosystems coated with a mesoporous silica shell (termed as Au-MSS) has attracted the scientific attention due to their advantageous properties for cancer therapy (Ghosh Chaudhuri and Paria, 2012). Mesoporous silica is a chemically inert material with large surface area, low cytotoxicity and also with a good colloidal stability. Moreover, silica surface can be

easily modified with different functional groups that would allow the tumor targeting or environmental responsiveness (Tarn et al., 2013). Additionally, the inclusion of mesoporous silica shell (MSS) on gold nanoparticles can improve their colloidal stability and also their biocompatibility by replacing the CTAB, which is known by its intrinsic cytotoxicity (Wu and Tracy, 2015).

In addition, apart from imaging capacity of gold nanostructures (e.g. CT imaging), the MSS pores can act as reservoirs for pharmaceutical agents, which is not feasible on bare gold nanostructures. In addition, fluorescent probes can also be loaded on the inner silica walls and enhance the imaging capacity of the particle (Figure 10) (Zhang *et al.*, 2013, Chen *et al.*, 2015, Song *et al.*, 2015). In this way, these material associations are great platforms to build theranostic nanocarriers, which combine in a single nanostructure both therapeutic and diagnostic functions (Figure 10) (Gautier et al., 2013).

The silica coating also enhances the thermal stability of gold nanoparticles, allowing the maintenance of the nanomaterials shape during the NIR light exposure and subsequent heating. This property allows gold nanostructures, such as gold NR, to maintain their NIR absorption and photothermal capacity after various NIR laser irradiation cycles (Figure 10) (Kanehara et al., 2009, Chen et al., 2013). Importantly, mesoporous silica is optically transparent to the NIR light, meaning that it does not compromise the therapeutic capacity of gold-based as photothermal agents (Ghosh Chaudhuri and Paria, 2012, Song et al., 2015). Therefore, the Au-MSSs allow the combination of chemo- and thermo- therapies to improve the therapeutic outcome, by attacking simultaneously different cancer pathways.

Furthermore, the thermotherapy can enhance the chemotherapeutics effect since this localized increase in temperature can induce cancer cell sensitization to chemotherapeutics action (thermosensitization) or even cause cellular damage and subsequent death if the temperature rises to values up to 45 °C. Moreover, the heat generated by the nanoparticles accumulated in the tumor can improve the blood flow in this local, which can further improve the nanoparticles accumulation in the tumor tissue (Issels, 2008, Sasidharan and Monteiro-Riviere, 2015).

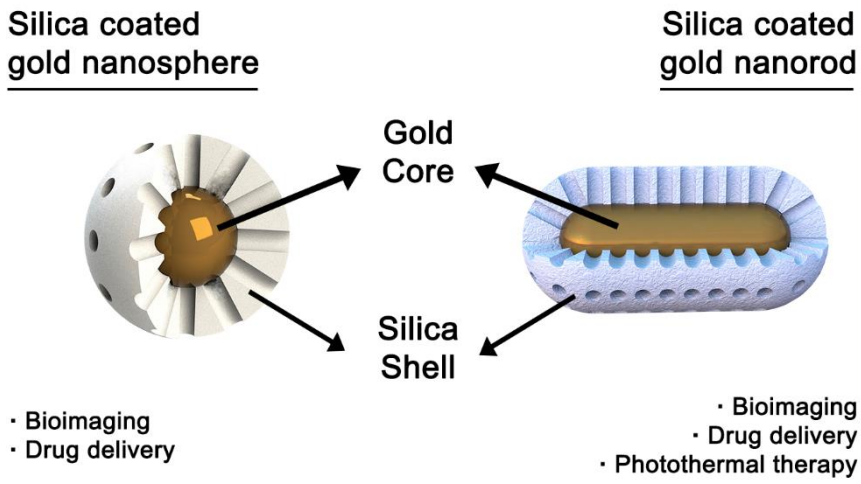

Figure 10 - Representation of silica coated gold nanoparticles structures.

Therefore, taking into account the Au-MSSs potential for cancer therapy and the fact that gold and silica are two of the few inorganic materials that have nanosystems with FDA approval for clinical trials in cancer therapy or imaging, is fundamental to further characterize their properties.

Aims

The main goal of this thesis was to compare the shape effect on the biological performance of gold core-mesoporous silica shell nanoparticles (Au-MSSs), particularly on the particle biocompatibility, cellular uptake and drug delivery capacity to cancer cells.

Therefore, the particular objectives include:

- → Synthesis, purification and characterization of Au-MSS spheres and rods;
- → Evaluation of drug loading capacity and release profile of the nanovehicles;
- → Evaluation of photothermal capacity;
- → Evaluation of nanoparticles biocompatibility;
- → Assessment of nanoparticles uptake by cancer cells;
- → Evaluation of nanoparticles cytotoxic activity (chemo and chemo-photothermal therapies).

Chapter 2

Materials and Methods

2. Materials and Methods

2.1. Materials

Hydrogen tetrachloroaurate (III) hydrate ($HAuCl_4$) was purchased from Alfa Aesar (Karlsruhe, Germany). Tetraethylorthosilicate (TEOS) and dimethyl sulfoxide (DMSO) were purchased from Acros Organics (Geel, Belgium). Hexadecyltrimethylammonium bromide (CTAB) was obtained from Tokyo Chemical Industry (Tokyo, Japan). Hydrochloric acid (HCl) was acquired from Panreac (Barcelona, Spain). Methanol was obtained from VWR International (Carnaxide, Portugal). L-ascorbic acid, silver nitrate ($AgNO_3$), Dulbecco's Modified Eagle Medium: nutrient mixture F-12 (DMEM-F12), Dulbecco's Modified Eagle medium-high glucose (DMEM-HG), resazurin, phosphate-buffered saline (PBS) solution, ethanol (EtOH), formaldehyde, paraformaldehyde, sodium borohydride ($NaBH_4$) and trypsin were purchased from Sigma–Aldrich (Sintra, Portugal). Primary normal human dermal fibroblast (FibH) cells were obtained from Promocell (Heidelberg, Germany) and human negroid cervix epithelioid carcinoma (HeLa) cells (ATCC® CCL-2™) were acquired from ATCC (Middlesex, United Kingdom). Hoechst 33342® and wheat germ agglutinin conjugate Alexa 594® (WGA-Alexa Fluor® 594) were purchased from Invitrogen (Carlsbad, California). Doxorubicin hydrochloride (Dox) was obtained from Carbosynth (Berkshire, United Kingdom). Fetal bovine serum (FBS) was acquired to Biochrom AG (Berlin, Germany). Cell imaging plates were acquired from Ibidi GmbH (Ibidi, Munich, Germany). Cell culture t-flasks were obtained from Orange Scientific (Braine-l'Alleud, Belgium).

2.2. Methods

2.2.1. Synthesis of Au-MSS spheres and rods

Au-MSS spheres were synthesized by adapting a method previously described in the literature (Chen *et al.*, 2013). Briefly, 0.05 g of CTAB and 0.60 mL of NaOH (0.50 M) were added to ultrapure water and left under stirring for 15 min. Afterward, 1.00 mL of formaldehyde (3.70 wt.%) and 0.80 mL of $HAuCl_4$ (0.05 M) were added to the previous solution. Subsequently, 0.91 mL of a solution of TEOS (33% v/v in ethanol) were added dropwise and left for 1 h under reflux conditions. The synthesized Au-MSS spheres were then recovered by centrifugation at 11,000 g and washed several times with ultrapure water.

Au-MSS rods were synthesized through a procedure that comprised three main steps (Nikoobakht and El-Sayed, 2003, Gorelikov and Matsuura, 2008). Initially, a seed solution was prepared by adding under stirring 0.60 mL of $NaBH_4$ (0.01 M) to an aqueous solution containing 5.00 mL of CTAB (0.20 M) and 5.00 mL of $HAuCl_4$ (0.50 mM). Subsequently, the grow solution was prepared by adding under stirring 0.21 mL of ascorbic acid (0.08 M) to an aqueous solution containing 15.00 mL of CTAB (0.20 M), 0.03 mL of $AgNO_3$ (0.10 M) and 0.30 mL of $HAuCl_4$ (0.05

M). Lastly, to produce the AuNRs, the seed solution (0.04 mL) was added to the growth solution and left at 30 ˚C for 16 h. The synthesis of the MSS was carried out by adapting the method described by Gorelikov and colleagues (Gorelikov and Matsuura, 2008). Initially, AuNRs were centrifuged (12,000 g for 20 min) to remove the excess of CTAB and resuspended in ultrapure water. Subsequently, 0.70 mL of CTAB (0.01 M) were added and left under stirring overnight. Afterwards, 0.07 mL of NaOH (0.10 M) were added to the solution and mixed for 30 min. Then, 0.03 mL of a solution of TEOS (20% v/v) in methanol were injected. This step was repeated three times with 30 min intervals and the solution was left under stirring for 24 h. The final solution was centrifuged at 18,000 g for 20 min and washed several times with ultrapure water to recover the Au-MSS rods.

2.2.2. Removal of surfactant template

The removal of the CTAB surfactant template was performed similarly for both nanoparticles by adapting a solvent based approach previously described by Moreira and co-workers (Moreira *et al.*, 2014). Briefly, the surfactant removal from Au-MSS rods and spheres was achieved by the sonication of the nanoparticles with a HCl solution (7.5% v/v in ethanol) for 10 min. Afterward, several washing steps with ethanol (100% v/v) were performed, in order to completely eliminate the CTAB residues. The final product was recovered by centrifugation (18,000 g for 15 min) and freeze-dried.

2.2.3. Characterization of nanocarriers physicochemical properties

2.2.3.1 Morphological characterization and size analysis

The morphology of both nanoparticles was analyzed through Transmission Electron Microscopy (TEM – Hitachi-HT7700, Japan). The nanoparticles samples were placed on formvar-coated copper grids and allowed to dry at room temperature. The images were acquired at an accelerating voltage of 100 kV. After image acquisition, the nanoparticles total size, silica shell thickness and gold core size were measured by using a specific software (Schneider *et al.*, 2012) (Image J 2.0.0, NIH Image, United States of America).

2.2.3.2. Zeta Potential analysis

The measurement of zeta potential of Au-MSS rods and spheres was determined by using a Zetasizer Nano ZS equipment (Malvern Instruments, Worcestershire, UK). In all the measurements, the nanoparticles were resuspended in ultrapure water. The data was collect at 25 ˚C in a disposable capillary cell at a detection angle of 173˚. Zeta potential of MSNs was calculated by using the Smoluchowski model (f(ka)=1.50) included in the Zetasizer software (v 7.03).

$$\zeta = \frac{U_E \, 3 \, \eta}{2 \, \epsilon \, f(ka)} \qquad (1)$$

Where ζ corresponds to zeta potential, U_E is the electrophoretic mobility, η corresponds to dynamic viscosity, ϵ represents the dielectric constant and f(ka) is the Henry's equation.

2.2.3.3. Ultraviolet-visible spectroscopy analysis

The success of Au-MSSs synthesis and the particle NIR absorption capacity was evaluated by UV-vis spectroscopy, using a Thermo Scientific Evolution™ 201 Bio UV-vis Spectrophotometer (Thermo Fisher Scientific Inc., Massachusetts, United States of America). The UV-vis spectra of Au-MSS spheres and rods were recorded at 300 nm/min scanning rate, with a wavelength range from 200 to 1100 nm.

2.2.3.4. Fourier transform infrared spectroscopy analysis

Fourier transform infrared (FTIR) spectroscopy was used to evaluate the compounds present in the samples. This data is important in order to confirm the successful formation of the MSS coating and also for verifying the purification step efficacy. The interferograms were recorded in a Nicolet iS10 spectrometer (Thermo Scientific Inc., Massachusetts, United States of America) acquiring 256 scans with a spectral resolution of 4 cm^{-1} ranging from 4000 cm^{-1} to 600 cm^{-1}. Moreover, in all the acquired data was performed a baseline correction and atmospheric suppression to avoid any possible interferences in the FTIR spectra. Data analysis was executed in the OMNIC spectra software (Thermo Scientific).

2.2.3.5. Nanoparticle porosity and surface area analysis

The porosity and surface area of Au-MSS nanoparticles was analyzed by acquiring the nitrogen sorption isotherms at -196.15 ˚C, using a Nova 2200e surface area and pore size analyzer (Quantachrome Instruments Corporate, Florida, United StatesUnite of America). Before the analysis, the sample were degassed under a flow of dry inert gas, during 24h. The adsorption isotherm was obtained by measuring the amount of gas adsorbed across a wide range of relative pressures at a constant temperature. On the other side, desorption isotherms are delineated by measuring the gas removed with the pressure reduction.

The nanoparticle surface area was calculated by the Brunauer–Emmett–Teller (BET) method using experimental points at a relative pressure of P/P_0 = 0.05–0.25.

$$\frac{1}{W((p_0/P)-1)} = \frac{1}{W_m C} + \frac{C-1}{W_m C}\left(\frac{P}{p_0}\right) \quad (2)$$

$$S_t = \frac{W_m N A_{CS}}{M} \quad (3)$$

Where W is the weight of gas adsorbed, P/P_0 the relative pressure, W_m the weight of adsorbate monolayer, C the BET constant, S_t the total surface area, N the Avogadro's number, M the molecular weight of adsorbate and A_{cs} the adsorbate cross-sectional area.

Porosity was determined by the Barrett–Joyner–Halenda (BJH) method and the pore volume was estimated from the amount of adsorbed nitrogen at the relative pressure of 0.99.

$$r_k(^{\circ}A) = \frac{4.15}{\log\frac{P_0}{P}} \quad (4)$$

$$r_p = r_k + t \quad (5)$$

Where $r_k(^{\circ}A)$ is the Kelvin radius of the pore, r_p the actual radius of the pore and t the thickness of the adsorbed film.

2.2.4. Drug loading

The Dox loading in Au-MSS rods or spheres was accomplished through the impregnation of the particles in a Dox solution. Briefly, Au-MSS rods or spheres were resuspended in 5.00 mL of PBS (pH 7.2) containing Dox (10% w/w). The solution was then sonicated for 15 min and stirred for 48 h at room temperature, in dark conditions. Afterward, the drug-loaded nanoparticles were recovered by centrifugation at 18,000 g, for 30 min and freeze-dried. The supernatant was stored to quantify the amount of drug loaded within nanocarriers.

The Dox content in the nanoparticles was calculated by measuring the supernatant absorbance at 485 nm, using a UV-vis Spectrophotometer (Thermo Scientific Evolution™ 201 Bio UV-Vis Spectrophotometer, Thermo Fisher Scientific Inc., United States of America), and a calibration curve (Abs = 19,323 C + 6E-05; r^2 = 0.9995). The encapsulation efficiency of Au-MSS rods or spheres was calculated through equation (6):

$$\text{Encapsulation efficiency } (\%) = \frac{\text{(Initial drug weight-Drug weight present in the supernatant)}}{\text{Initial drug weight}} \times 100 \quad (6)$$

2.2.5. *In vitro* drug release

The characterization of the drug release profile was performed according to a method previously described in the literature (de Melo-Diogo *et al.*, 2014). Briefly, the Au-MSS rods or spheres were resuspended in PBS and inserted in a Float-A-Lyzer dialysis bag with a molecular cut-off of 1000 Da. The dialysis was performed at 37 °C under magnetic stirring in 10 mL of PBS solution, at pH 5.6 or 7.4. At different time points, 1 mL of samples were collected and the same volume of fresh PBS was added to the dialysis medium, in order to maintain the PBS volume. The Dox content was measured by the above-described UV-vis method.

2.2.6. Evaluation of the *in vitro* photothermal capacity of the nanoparticles

The *in vitro* photothermal capacity of Au-MSS rods or spheres was performed as previously reported in the literature (Liu *et al.*, 2015c). Briefly, Au-MSS rods or spheres at different concentrations were irradiated with a NIR laser (808 nm, 1.7 W/cm^2). The temperature

variation of the solution was measured at different time points (from 1 up to 10 min) by using a thermocouple sensor with an accuracy of 0.1 °C. A control group without the particles was also irradiated and the temperature changes were monitored.

2.2.7. Nanoparticles biocompatibility assays

The Au-MSS spheres and rods biocompatibility was characterized by incubating the nanomaterials with HeLa or FibH cells. The 3-(4, 5-dimethylthiazolyl-2)-2,5-diphenyltetrazolium bromide (MTT) assay was performed to characterize cells viability in the presence of nanomaterials. The HeLa and FibH cells were seeded into a 96-well flat bottom culture plates at a density of 10,000 cells per well, with 200 µL of medium (DMEM-HG and DMEM-F12 medium, respectively). During 24 h, cells were cultured at 37 °C in a humid atmosphere containing 5% CO_2. After this period, the cells were incubated with different concentrations of Au-MSS rods or spheres, from 20 to 100 µg/mL. After 24, 48 and 72 h of exposition, the mitochondrial redox activity was assessed through the MTT reduction (Ribeiro *et al.*, 2009). Briefly, the medium was removed and 50 µL of MTT solution (5 mg/mL) were added to each well. After 4 h of incubation, the solution was removed and 200 µL of DMSO were added to dissolve the resulting crystals. The reduction of MTT to its insoluble formazan product was then quantified by measuring the sample absorbance at 570 nm using a microwell plate reader (Sunrise-Basic TECAN, Männedorf, Switzerland). Cells incubated with EtOH (70% v/v) were used as positive control (K^+), whereas cells without being incubated with nanomaterials were used as negative control (K^-).

2.2.8. Evaluation of the nanoparticle cellular uptake

The Au-MSSs cellular uptake by HeLa cells was characterized through confocal laser scanning microscopy (CLSM), followed the protocol previously described in (Gaspar *et al.*, 2015) and by taking advantage of Dox autofluorescence to track the nanoparticles fate.

For the analysis of the nanoparticles cellular uptake, 20,000 HeLa cells were seeded in µ-Slide 8 well Ibidi imaging plates (Ibidi GmbH, Germany) and incubated for 24 h, at 37 °C in a humidified atmosphere with 5% CO_2. Afterward, cells were incubated with Au-MSS rods or spheres during 1 or 4 h. Subsequently, the seeded cells were washed with PBS, fixed with paraformaldehyde (4%) for 15 min and rinsed with PBS. For cell cytoplasm staining, cells were treated with WGA-Alexa Flour® 594 whereas the cell nucleus was labeled with Hoechst 33342®. The CLSM images were then acquired with a Zeiss LSM 710 Confocal microscope (Carl Zeiss SMT Inc., Germany) equipped with a Plan Apochromat 63x/1.4 Oil Differential Interference Contrast (DIC) objective. Successive z-stacks were also acquired and the 3D reconstruction and analysis of the confocal images were performed in the Zeiss Zen 2010 software.

2.2.9. Characterization of the cytotoxic profile of the nanoparticles

To evaluate the NIR-induced cytotoxic activity of the Au-MSSs, different particle conditions were incubated with HeLa cells in the presence or absence of NIR laser irradiation. Briefly, the cells were seeded into a 96-well flat bottom culture plates at a density of 10,000 cells per well using the same culture condition that was previously described. After 24 h of culture, the HeLa cells were incubated with the different particle formulations (Dox loaded in Au-MSS rods or spheres) or free Dox (in a similar concentration to that loaded on particles). After 6 h, some of the test conditions were irradiated using a laser (808 nm, 1.7 W/cm^2 for 5 min) to evaluate the Au-MSSs NIR-induced cytotoxic effect. During the laser irradiation cycles, the temperature of the cell culture plates was maintained close to 37 °C by using a heating mantle. After 24 h of incubation, the cell viability was determined by using the MTT assay as previously described. The cell viability in each group was expressed as a percentage in comparison to the negative control (K^-, i.e. cell without particles incubation), whereas cells incubated with EtOH (70% v/v) were used as positive controls (K^+).

2.2.10. Statistical analysis

All data are presented as mean ± standard deviation (s.d.). One-way analysis of variance (ANOVA) with the Student–Newman–Keuls post-test was used to compare the results obtained for the different groups. A p value lower than 0.05 was considered statistically significant. Statistical analysis was performed using GraphPad Prism v.6.0 software (Trial version, GraphPadSoftware, California, United States of America).

Chapter 3

Results and Discussion

3. Results and Discussion

3.1. Synthesis of nanoparticles

Core-shell-based nanoparticles are promising multidisciplinary platforms for cancer therapy and diagnosis. The nanoparticles organization in core-shell structures is a simple approach that allows the combination of different functions, such as drug delivery, PTT, targeting and imaging, in a single system (Ghosh Chaudhuri and Paria, 2012). Moreover, the combination of gold and silica materials has attracted the attention of the scientific community due to their unique and versatile properties, that are advantageous in cancer-related applications. Gold nanoparticles have facile surface functionalization, a great colloidal stability and inertness (Sasidharan and Monteiro-Riviere, 2015). Further, gold nanoparticles have been already applied as photothermal and imaging agents, radiosensitizers or even as drug delivery systems. On the other side, silica-based materials, principally those with mesopores, provide a stable and rigid framework resistant to adverse conditions (e.g. enzymes, heat, mechanical stress and pH) that can encapsulate both hydrophobic and hydrophilic drugs (Kango *et al.*, 2013). Therefore, the addition of a MSS to gold nanoparticles could allow the combination of chemo- and photothermal therapies to potentiate nanomaterials therapeutic effect, while simultaneously improve the biocompatibility and stability of gold nanoparticles. However, the effect of the Au-MSSs shape on the nanoparticles interaction with cells, uptake and cytotoxic ability, is still unclear. Huang and colleagues reported that silica mesoporous nanoparticles with a rod-like structure are more uptaken than those with spherical shape. In contrast, Arnida and coworkers observed that gold-based nanoparticles with spherical shape have a higher uptake by macrophage cells than the gold NRs (Huang *et al.*, 2010, Janát-Amsbury *et al.*, 2011).

The Au-MSS systems produced in this work were synthesized by adapting methods previously described in the literature. The Au-MSS spheres were synthesized in an one-pot protocol, accordingly to a method proposed by Chen and colleagues (Chen *et al.*, 2013). Initially, an alkaline solution containing CTAB molecules was prepared. Then, the gold precursor ($HAuCl_4$) is reduced by formaldehyde, in order to originate CTAB-stabilized gold nanosized spheres. Subsequently, the silica shell was produced by adding TEOS, which is hydrolyzed and forms a mesoporous shell around gold nanoparticles. At this point, CTAB works as a pore template surfactant for TEOS condensation around the gold cores and, thus, leads to the formation of core-shell based nanostructure.

In contrast, gold NR were obtained through a seed-mediated growth method. Gold NR nucleus was obtained according to the protocol described by Nikoobakht (Nikoobakht and El-Sayed, 2003), whereas the MSS coating was achieved by a method described by Gorelikov and Matsuura (Gorelikov and Matsuura, 2008). Initially, small CTAB-stabilized gold nanoparticles were produced through the reduction of $HAuCl_4$ by sodium borohydride, resulting in a so-called seed

solution. Subsequently a growth solution was prepared by adding ascorbic acid (a reducing agent) to a solution containing silver and gold ions in the presence of CTAB. In this solution, the gold source is reduced from Au III to Au I. Then, the seed solution is added to the growth solution and the small gold nanoparticles (i.e. seeds) catalyze the complete reduction of gold (Au I to Au atom) on their surface by ascorbic acid. Subsequently, the gold atoms will grow on the surface of seed nanoparticles leading to the formation of the gold NR. The CTAB during this process acts both as stabilizer agent as well as template agent. The silver nitrate present in the growth solution allows the tuning of the gold NR aspect ratio, due to the formation of AgBr complex (Br^- coming from CTAB) on the nanoparticle surface that directs the growth of the NR (Pérez-Juste *et al.*, 2005, Scarabelli *et al.*, 2015). After the gold NR core formation, the silica shell was formed by promoting the TEOS hydrolysis and consequently its condensation on gold NR surface, using the CTAB as a pore structuring template (Gorelikov and Matsuura, 2008).

Therefore, from a scale up potential, it is important to notice that the observed differences in the synthesis procedures can greatly impact on the translation of these technologies to the industry. In particular, the rod-shaped particles present a more laborious and time-consuming synthesis process, comprised of three individual steps, namely, synthesis of seeds solution, followed by gold NR grow and finally, silica shell coating. Thus, it is required more than one day to obtain the final product. On the other hand, the Au-MSS spheres are produced through a simpler process, based on a one-step synthesis procedure, that only takes about 2 h to occur. Such differences between the two methodologies make the Au-MSS spheres a more desirable platform when the production scale up is intended.

3.2. Size and zeta-potential characterization of nanoparticles

The analysis of the TEM images confirmed the successful synthesis of Au-MSSs and the nanoparticle organization in a single gold core with a uniform silica shell (Figure 11 A and B). Moreover, it is also perceptible in the close-up TEM images the porous structure of MSS for both nanosystems. The particle size measurements revealed that Au-MSS spheres were slightly larger than their counterparts (Table 1). Au-MSS spheres are comprised of a gold core of 20 ± 4 nm and a silica shell with 45 ± 4 nm of thickness resulting in a particle with the total size of 109 ± 8 nm. In contrast, the Au-MSS rods possessed an average length of 70 ± 11 nm and a width of 47± 7 nm (approximately 70 x 47), being comprised of a gold NR core with an aspect ratio of 3.4 and a MSS with 18 ± 2 nm in thickness.

Moreover, the Au-MSSs size distribution by intensity reveals a unique and uniform population of nanoparticles (Figure 12 A and C).The displayed particle sizes are in concordance with similar reports found in the literature, concerning the formation of uniform MSS on a gold core surface (Gorelikov and Matsuura, 2008, Wu and Tracy, 2015). For example, Song and colleagues reported the production of highly uniform nanoparticles for imaging purpose comprised by a 20 nm spherical gold core and 45 nm shell such as Au-MSS spheres (Song *et al.*, 2015). Further,

Zhang and colleagues developed an Au-MSS rod-based system with an identical shell thickness (16 nm) but with a smaller width size for thermal- and chemotherapy towards HeLa cells (Zhang *et al.*, 2015).

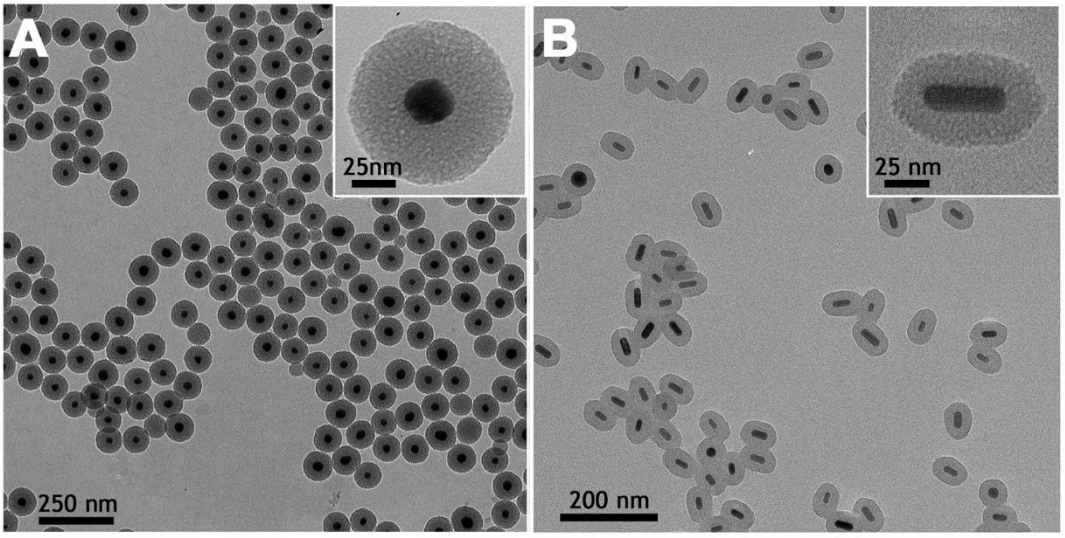

Figure 11 - Size and morphology characterization of Au-MSSs. TEM images of the Au-MSSs spheres (A) and rods (B).

The observed differences in Au-MSSs size and shape can affect the performance of the nanoparticle. Besides, the displayed sizes allow the nanoparticles to exploit the well-known EPR effect that is found in tumor tissue due to the irregular tumor vasculature (blood vessels present fenestrae with 400 – 500 nm) and impaired lymphatic drainage (Xu *et al.*, 2015). Additionality, the observed differences in the shell thickness can be an important parameter that affects the particles capacity to encapsulate bioactive molecules, since silica pores will be the drug reservoirs of the particles (Jia *et al.*, 2013b).

Furthermore, the zeta potential analysis revealed differences in the particle charge (Table 1 and Figure 12 B and D). The spheres, which have a higher shell thickness, displayed a zeta potential of -16 ± 1 mV. In turn, the rods exhibited a zeta potential of -12 ± 1 mV. The obtained data indicates that the thickness of the silica shell significantly impacts on the nanoparticle charge, which can be justified by the negatively charged silanol groups present on MSS surface. Moreover, these values are in accordance with previously reports where similar gold and silica-based delivery systems were produced (Luo *et al.*, 2014, Mekaru *et al.*, 2015, Sadeghnia *et al.*, 2015, Zhang *et al.*, 2015). Zeiderman and coworkers reported a similar zeta potential (i.e. -11 mV) to Au-MSS rods by using a gold NR core with a similar aspect ratio and slightly thicker MSS (Zeiderman *et al.*, 2016). Moreover, Zhang and colleagues developed an Au-MSS rod based system that comprised a smaller gold core, that leads to a more negative zeta potential (-19 mV) (Zhang *et al.*, 2015).

Table 1 - Size and charge characterization of Au-MSSs. Data are presented as mean ± s.d. (n ≥ 300).

		Size (nm)			Zeta Potential (mV)
		Total	Gold Core	Silica Shell	
Au-MSS spheres		109 ± 8	20 ± 4	44.9 ± 3.7	-16 ± 1
Au-MSS rods	**Lenght**	70 ± 10	38 ± 6	17.9 ± 2.2	-12 ± 1
	Width	47 ± 7	11 ± 2		

As above mentioned, the zeta potential is an important parameter that affects the nanoparticles interaction with the biological components. The nanosystems circulation time, penetration in tumor and their interactions with cells are highly influenced by zeta potential. The neutral charge (zeta potential of ±10 mV) is considered ideal for nanoparticles circulation in the human body (Ernsting *et al.*, 2013). Taking this into account, the Au-MSS rods seems to possess the most appropriated zeta potential value, since their surface charge is less negative than the spherical ones.

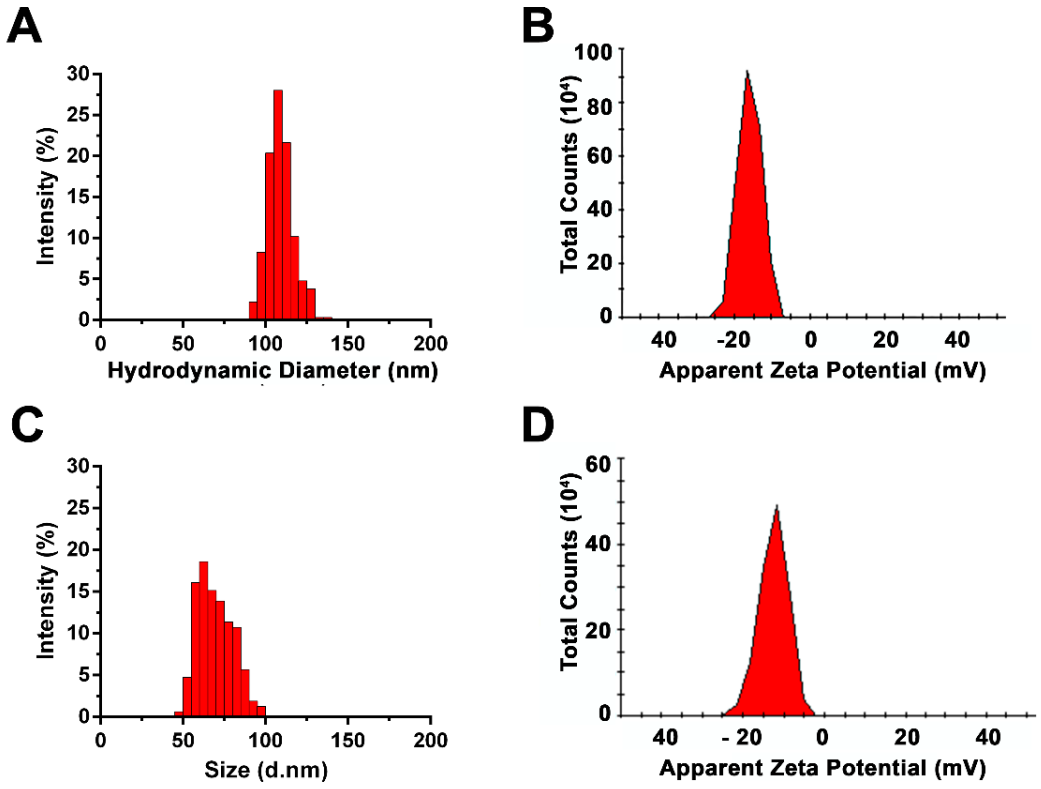

Figure 12 - Size and charge characterization of Au-MSSs. Size distribution by intensity of Au-MSS spheres (A) and rods (C). Zeta potential measurements of Au-MSS spheres (B) and rods (D).

3.3. Fourier transform infrared spectroscopy analysis

The FTIR characterization of the nanosystems was carried out for assessing the formation of the silica coating and to characterize the efficacy of the purification procedure (Figure 13). The presence of the silica shell on Au-MSSs was confirmed by the presence of the three characteristic peaks in the 1100 to 750 cm^{-1} region, that belong to the Si-O, Si-O-Si and Si-OH vibrations (Zhang *et al.*, 2015). Moreover, after the nanoparticles formation a purification step is required due to the use of the highly toxic CTAB surfactant (CTAB has been shown to be capable of damaging biological membranes and cause the release of intracellular enzymes) (Sharif, 2012). The FTIR spectrum analysis of Au-MSS rods and spheres with the CTAB template (Figure 13) presented the characteristic peaks of the CTAB molecule, two absorption bands between 2950 cm^{-1} and 2850 cm^{-1} that belong to the C–H stretching vibrations, and a C-H deformation around the 1500 cm^{-1}. After the purification procedure, the FTIR spectra of the Au-MSSs revealed that the C–H stretching vibration bands and C-H deformation disappear. Thereby, this results showed that the CTAB is completely removed from the samples, which may contribute to the system biosafety and biocompatibility.

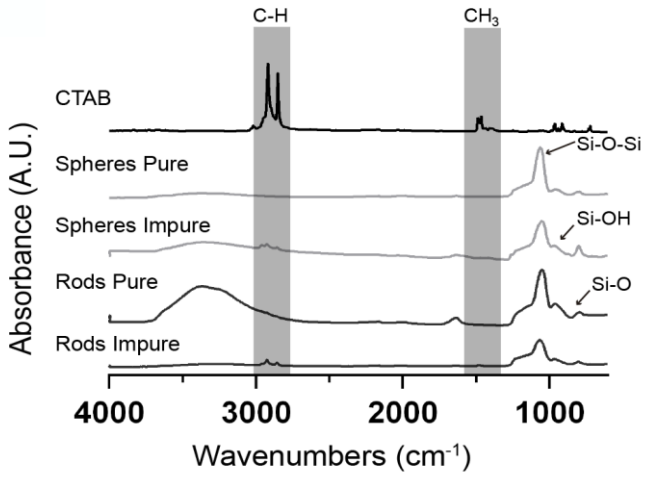

Figure 13 - Physicochemical characterization of Au-MSSs. FTIR spectra of CTAB, Au-MSS spheres (Pure and Impure) and rods (Pure and Impure).

3.4. Porosity and surface area analysis of the nanoparticles

The Au-MSSs surface area and pore size measurements were performed by analyzing the nitrogen adsorption/desorption isotherms. The adsorption isotherm is obtained by measuring the amount of gas adsorbed with the increase of the relative pressure at a constant temperature, whereas the desorption isotherm refers to the amount of gas that is released as the pressure decreases. These experiments provide information about nanoparticle surface area and pore volume and diameter. Such data can be used to confirm the CTAB template removal and also predict the drug loading capacity of Au-MSSs.

An initial analysis of the Au-MSSs adsorption/desorption isotherms shows that both rods and Au-MSS spheres possess type IV isotherms (Figure 14) (ALOthman, 2012). This indicates that the particles possess a mesoporous structure with pore sizes in the range on 1.5 - 100 nm.

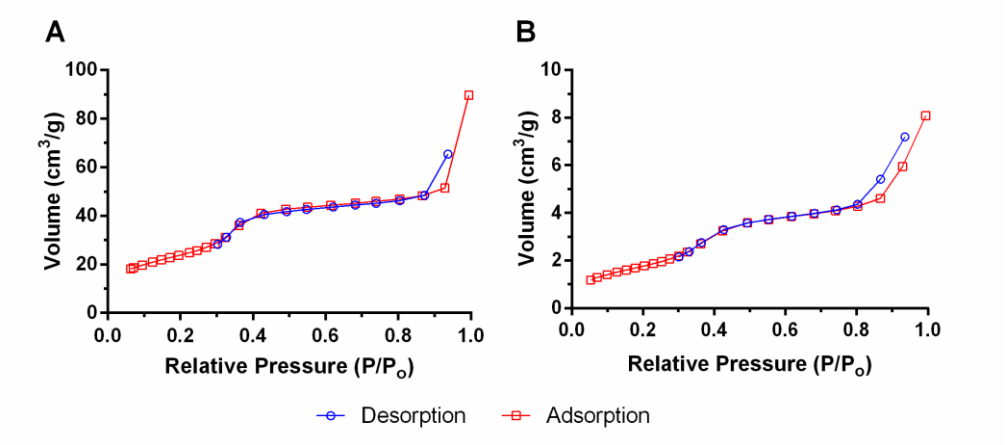

Figure 14 - Representation of nitrogen adsorption and desorption isotherms of Au-MSS spheres (A) and rods (B).

Moreover, by applying the BJH analysis to the adsorption/desorption isotherms it is possible to determine that both Au-MSSs possess an identical pore diameter, around 3.2 nm (Table 2). These results are in agreement with those reported in literature (Moreira *et al.*, 2014). Further, the BJH analysis revealed that the Au-MSS spheres possessed a higher pore volume than the rods counterparts, 0.8 and 0.5 cm^3/g, respectively. This increased pore volume can be justified by the Au-MSS spheres higher shell thickness and consequently pores with increased length. Such result indicates that the Au-MSS spheres possess a higher capacity to encapsulate therapeutic molecules and therefore may be capable of deliver higher drug payloads to cancer cells. Furthermore, the Au-MSS spheres also showed an increased specific surface area than the rods counterparts (716.7 and 339.8 m^2/g). Such difference can be correlated to the higher pore length of the spherical nanoparticles, which will greatly increase the overall nanoparticle surface area. The porosity analysis is in concordance with similar core-shell silica-based nanosystems with a spherical or rod-like shape (Shen *et al.*, 2013, Wang *et al.*, 2014, Zhang *et al.*, 2015, Yu and Zhu, 2016).

Table 2 - Porosity and surface analysis of Au-MSSs after being purified.

	Surface Area (m^2/g)	Pore Diameter (nm)	Pore Volume (cm^3/g)
Au-MSS Spheres	716.7	3.2	0.8
Au-MSS Rods	339.8	3.2	0.5

3.5. UV-vis spectroscopy and photothermal capacity analysis

The UV-vis absorbance spectrum of Au-MSSs was acquired to confirm the success of the synthesis procedure. Gold nanospheres show one absorption band, while NRs have two characteristic absorption bands, the transverse and the longitudinal plasmon resonances (Huang *et al.*, 2008).

The UV-vis spectrum of Au-MSS spheres (Figure 15 – gray line) shows a peak at 550 nm, which is coherent with the data presented in the literature for gold spheres with similar sizes (Jain *et al.*, 2006). On the other hand, the Au-MSS rods displayed two different absorption peaks at 500 nm and 770 nm (Figure 15 – black line). The first peak is attributed to the transverse plasmon resonance of the particles, whereas the peak at 770 nm is assigned to the longitudinal plasmon resonance. The presence of these two different peaks in the UV-vis absorbance spectrum is consistent with that reported in the literature for other AuNRs coated with a silica shell and with a similar aspect ratio (Alkilany *et al.*, 2009, Huang and El-Sayed, 2010, Zhang *et al.*, 2015).

Moreover, the Au-MSS rods display a strong absorption in the 700-900 nm range, a wavelength interval where the biological components present a low or insignificant absorption, thus making these systems suitable for PTT or light triggered drug delivery (Liu *et al.*, 2016).

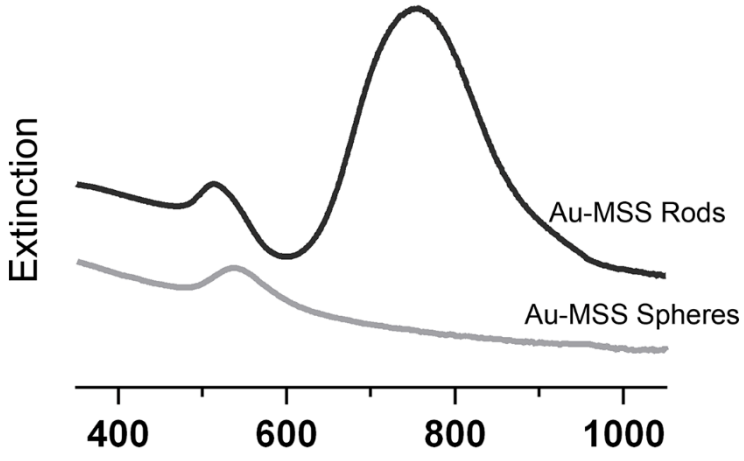

Figure 15 - Physicochemical characterization of Au-MSSs. The UV-vis spectra of Au-MSS spheres and rods nanoparticles.

The successful application of nanomaterials in cancer PTT is dependent on their capacity to absorb and convert NIR light into heat, sensitizing cells to the drugs action or promoting cell apoptosis (Krishnan *et al.*, 2010, Chatterjee *et al.*, 2011).

For this purpose, both formulations were exposed to 808 nm NIR light for 1 up to 10 min and the temperature variations were recorded (Figure 16 A). Au-MSS spheres at the tested concentrations (50 and 100 µg/mL) only promoted an increase in temperature of 2 to 4 °C,

after 10 min of irradiation. This result is in agreement with the optical properties displayed by these particles, since they have almost no absorption in the NIR region. In contrast, the Au-MSS rods, which have a high NIR absorption, caused a temperature increase of 20 ˚C (100 µg/mL of Au-MSS rods) and 15 ˚C (50 µg/mL of Au-MSS rods) after the same period of irradiation. The obtained results are consistent with those available in the literature for similar gold-silica-based nanosystems (Zhang *et al.*, 2015). Liu and colleagues reported a similar NIR-induced heating profile by using silica-coated AuNRs, although they used a lower laser power density (1 W/cm^2) and higher particle concentration (Liu *et al.*, 2015a). Moreover, Au-MSS rods (100 µg/mL) induced a temperature variation (ΔT = 15 ˚C) that can lead to cellular damage (usually attained for a temperature above 45-50 ˚C) with 5 min NIR irradiation (Mallick *et al.*, 2013). Therefore, this exposition time was selected for subsequent biological studies.

Additionally, the Au-MSS spheres and rods also demonstrated a good photothermic stability since, the Au-MSSs exposition to multiple irradiation cycles did not provoke changes in the photothermal capacity of the nanoparticles (Figure 16 B). Such result can be explained by the silica coating that stabilizes and protects the gold cores from premature degradation, thus allowing these nanomaterials to support multiple irradiation cycles without sacrificing their heat conversion capacity (Chen *et al.*, 2010). Moreover, the different Au-MSSs heating profile demonstrates how the nanoparticle shape can induce changes in the nanoparticles properties, supporting the importance of fully characterize this particle parameter for each nanoparticle-based system.

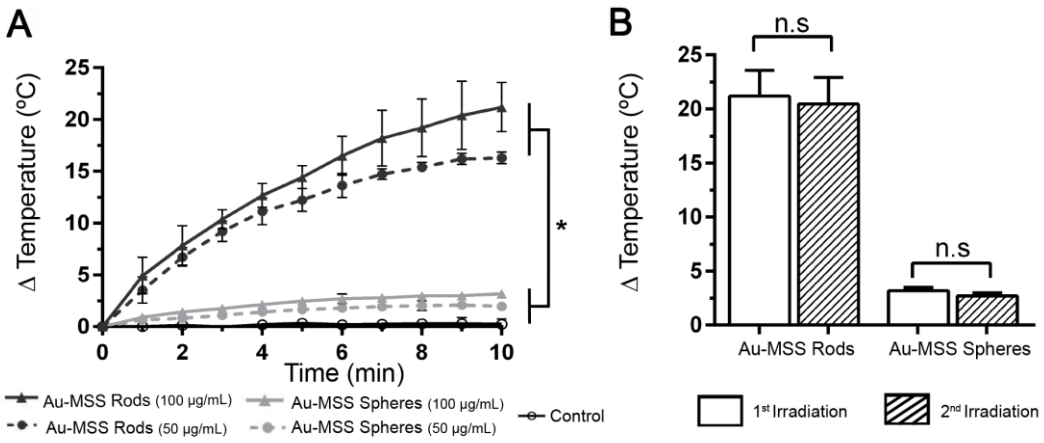

Figure 16 - *In vitro* evaluation of the Au-MSSs photothermal capacity. (A) Temperature variation curves when different Au-MSSs concentrations are irradiated with NIR light (808 nm, 1.7 W/cm^2, 10 min). (B) Temperature variation for Au-MSSs (100 µg/mL) after 1 or 2 cycles of NIR laser irradiation (808 nm, 1.7 W/cm^2, 10 min) after 1 or 2 cycles of irradiation. Data are presented as mean ± s.d., *p<0.05, n= 3.

3.6. Drug loading and release profile analysis

The Au-MSSs potential to encapsulate bioactive molecules was assessed by using Dox as drug model, a hydrophilic compound broadly used in first-line chemotherapy. The drug loading was achieved by dispersing the Au-MSS rods or spheres in a Dox solution for 48 h (Figure 17 A). During this process, the positively charged Dox molecules will diffuse into the MSS pores and interact with the negatively charged silanol groups present on the silica shell, being confined to the particles interior. The Au-MSSs were then recovered by centrifugation and the amount of Dox encapsulated within the particle was quantified by measuring the supernatant absorbance at 485 nm by using a Dox calibration curve (Figure 17 B).

The obtained encapsulation efficiencies for both Au-MSS rods and spheres demonstrate the particles capacity to retain the drugs within its pores. The loading results showed that Au-MSS spheres can encapsulate a higher content of Dox, around 80 µg of drug per 1 mg of Au-MSSs, while Au-MSS rods only retained 52% of the initial drug (i.e. 52 µg Dox per 1 mg of Au-MSSs) (Figure 17 C). Such results can be justified by the shell thickness differences displayed by the spheres and the rods. The increased shell thickness on Au-MSS spheres originate mesopores with increased length and consequently possess a higher volume to incorporate Dox within MSS structure.

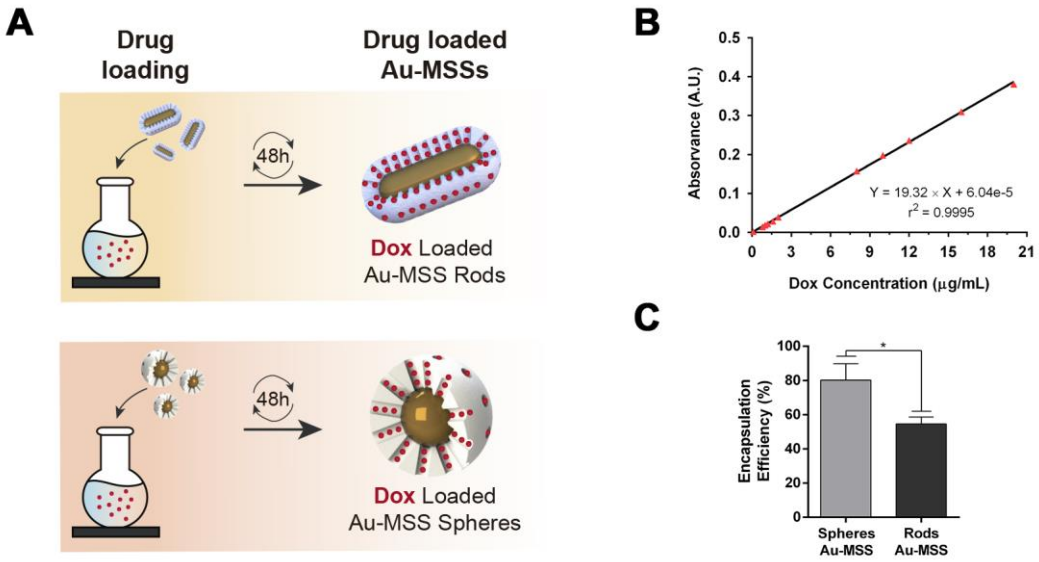

Figure 17 - Characterization of Dox encapsulation efficiency of Au-MSSs. (A) Schematics of the drug loading. (B) Standard curve (Abs = 19.32 C + 6E-5; r^2 = 0.9995) of Dox in PBS. (C) Dox encapsulation efficiency of Au-MSS spheres and rods. Data are presented as mean ± s.d., n=3. The statistical analysis was performed by using t-Student test, with *p<0.05.

After the Dox loading, the release profile of the Au-MSS rods or spheres was characterized at two pH values, 5.6 (to simulate the tumor microenvironment and lysosomal compartments) and 7.4 (to simulate physiological conditions) (Figure 18 A and B). The obtained results (Figure 18 C and D) show that the release profile is not significantly affected by the pH variation.

Moreover, it was also possible to observe that Au-MSS rods release the Dox more rapidly (about 60%, for both pHs) than their counterparts. Such results may be correlated with the smaller shell thickness of Au-MSS rods and consequent smaller pore lengths. Thus drugs have a smaller path to travel and also less electrostatic interactions with pore wall. Moreover, both Au-MSS rods and spheres showed a release profile divided into two phases, an initial burst followed by a sustained release during the time of the experiment, which is usually observed for mesoporous silica nanoparticles (Wang, 2009). Such release profile is attributed to the physical and chemical entrapping of the drug within the MSS pores resulting in an initial burst release due to a higher concentration gradient between the particle pores and the release medium that tends to stabilize along time (Siepmann and Siepmann, 2008, Wang, 2009).

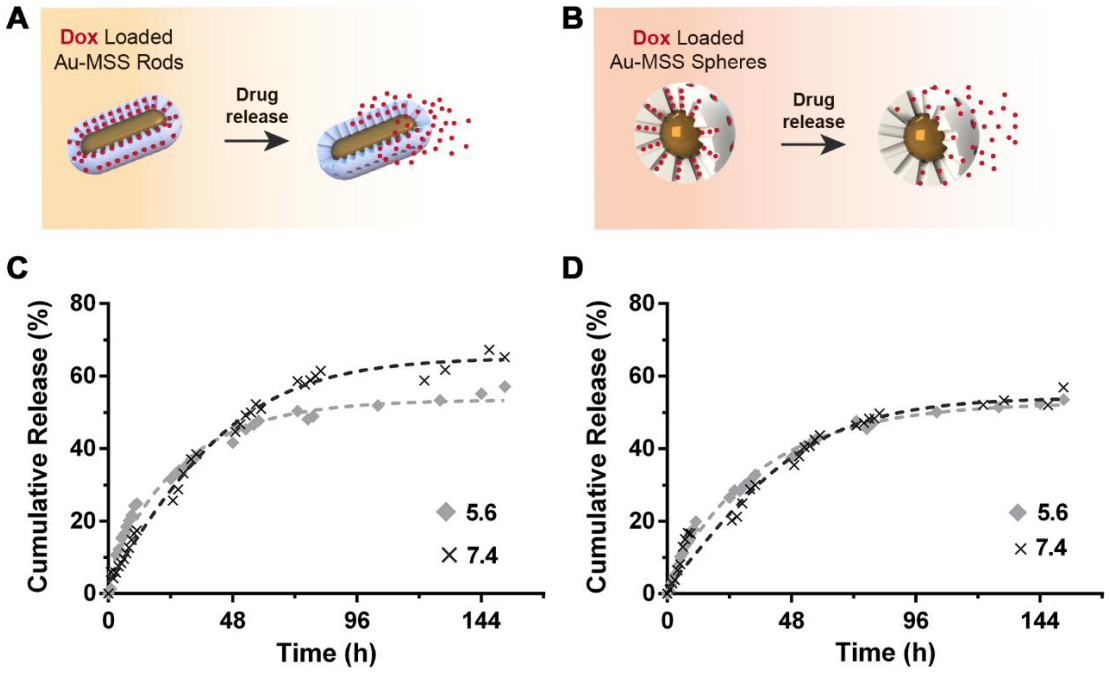

Figure 18 - Characterization of the release profile of Dox loaded Au-MSSs. Schematics of the release procedures of Au-MSS (A) rods and (B) spheres. Dox cumulative release at pH 5.6 and 7 of Au-MSS (C) rods and (D) spheres. Data are presented as mean ± s.d., *p<0.05, n=3.

3.7. Characterization of nanoparticles biocompatibility

The Au-MSSs biocompatibility was evaluated by using two cell lines, HeLa and FibH cells. In Figure 19 A and B it is possible to observe that both systems were biocompatible when incubated with HeLa cells at 24, 48 and 72 h and also for all the tested material concentrations (20 to 100 µg/mL). Moreover, Au-MSS rods and spheres did not reveal any toxicity towards non-cancer human cells (FibH) (Figure 19 C and D). Such results are in agreement with the different reports available in the literature for gold-silica-based nanosystems (Tang *et al.*, 2012, Mallick *et al.*, 2013, Shen *et al.*, 2013).

Additionally, in literature it is described that the length of Au-MSS rods can impact on the integrity of the cellular membrane and cytoskeleton leading to the disruption of the cell membrane and consequently to its death (Huang *et al.*, 2010). The biocompatibility assays performed herein showed that the Au-MSS rods presented a biocompatibility profile similar to the spherical Au-MSSs, which indicates that no significant alterations are being promoted on the cell membrane or cytoskeleton. Thus, the obtained results demonstrate that for the tested concentrations the shape does not influence the particle biocompatibility.

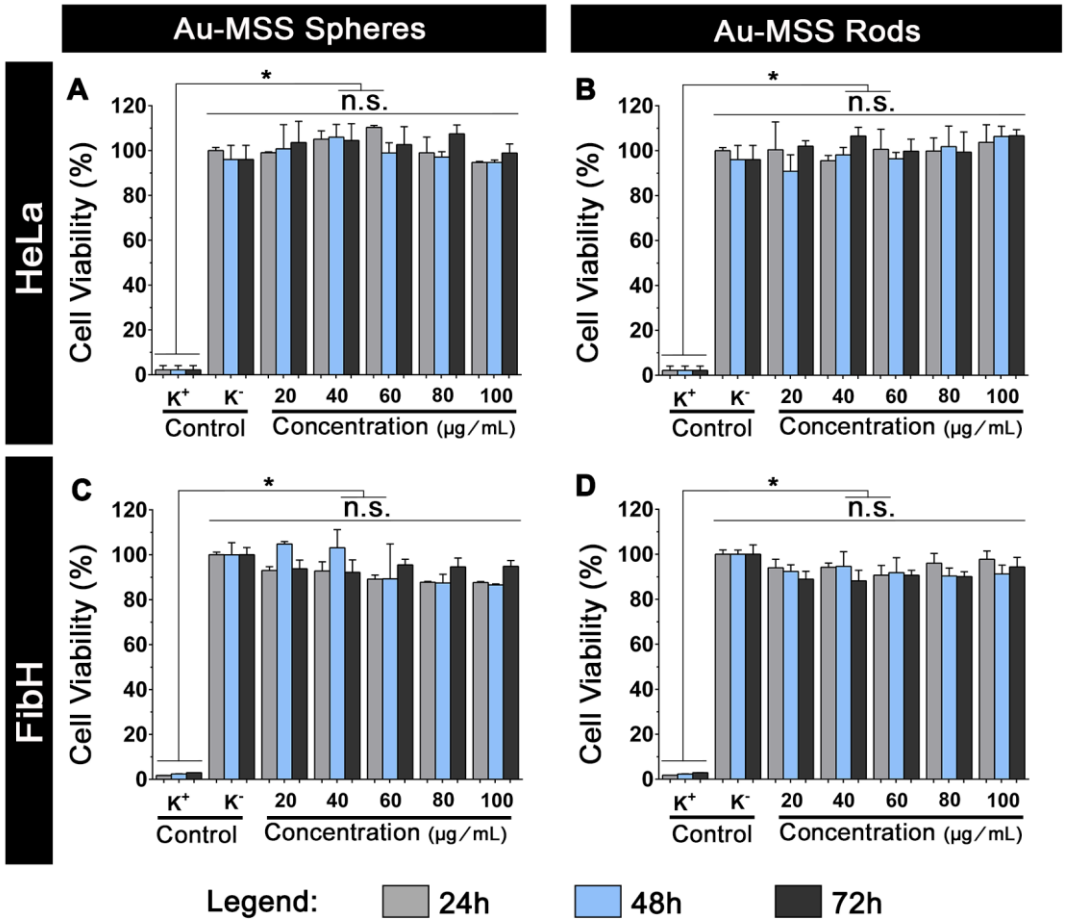

Figure 19 - Evaluation of the biocompatibility of Au-MSS spheres and rods at 24, 48 and 72 h in cancer (HeLa) and non-cancer (FibH) cells. (K^+): cells treated with ethanol; (K^-): cells without nanoparticles incubation. Data are presented as mean ± s.d., *$p<0.05$, n = 5.

3.8. Evaluation of the nanoparticle cellular uptake

After assessing the biocompatibility of the Au-MSS nanosystems, the cellular uptake by HeLa cells was evaluated by confocal laser microscopy. The tracking of Au-MSS nanoparticles was achieved by taking advantage of the autofluorescence of Dox molecules encapsulated within the particles. In Figure 20, it is possible to observe the Dox presence inside the HeLa cells, particularly, in the cell cytoplasm. Moreover, the Dox content inside the cells increased along time, being observed a clear increase in Dox fluorescence from 1 to 4 h of incubation.

Altogether, this data indicates that Au-MSSs were internalized by HeLa cells and were also able to deliver its content in the cell cytoplasm to exert the desired therapeutic effect, thus avoiding the premature drug degradation in the extracellular medium.

Furthermore, the Dox mean fluorescence intensity (MFI), 4 h after the nanoparticles incubation, was measured to compare the drug delivery efficacy of Au-MSS rods or spheres (Figure 21 A and B). Interestingly, after 4 h, the cells treated with Au-MSSs presented a superior Dox MFI than the free Dox-treated group. This *in vitro* increase of Dox accumulation in cancer cells by the use of nanoparticles is in agreement with other reports (Li et al., 2013, Gaspar et al., 2015). Such improved efficacy displayed by nanoparticles in *in vitro* assays has been attributed to the nanoparticles capacity to bypass different cellular drug efflux pathways or even drug degradation events that limit the drug dose that reaches cells.

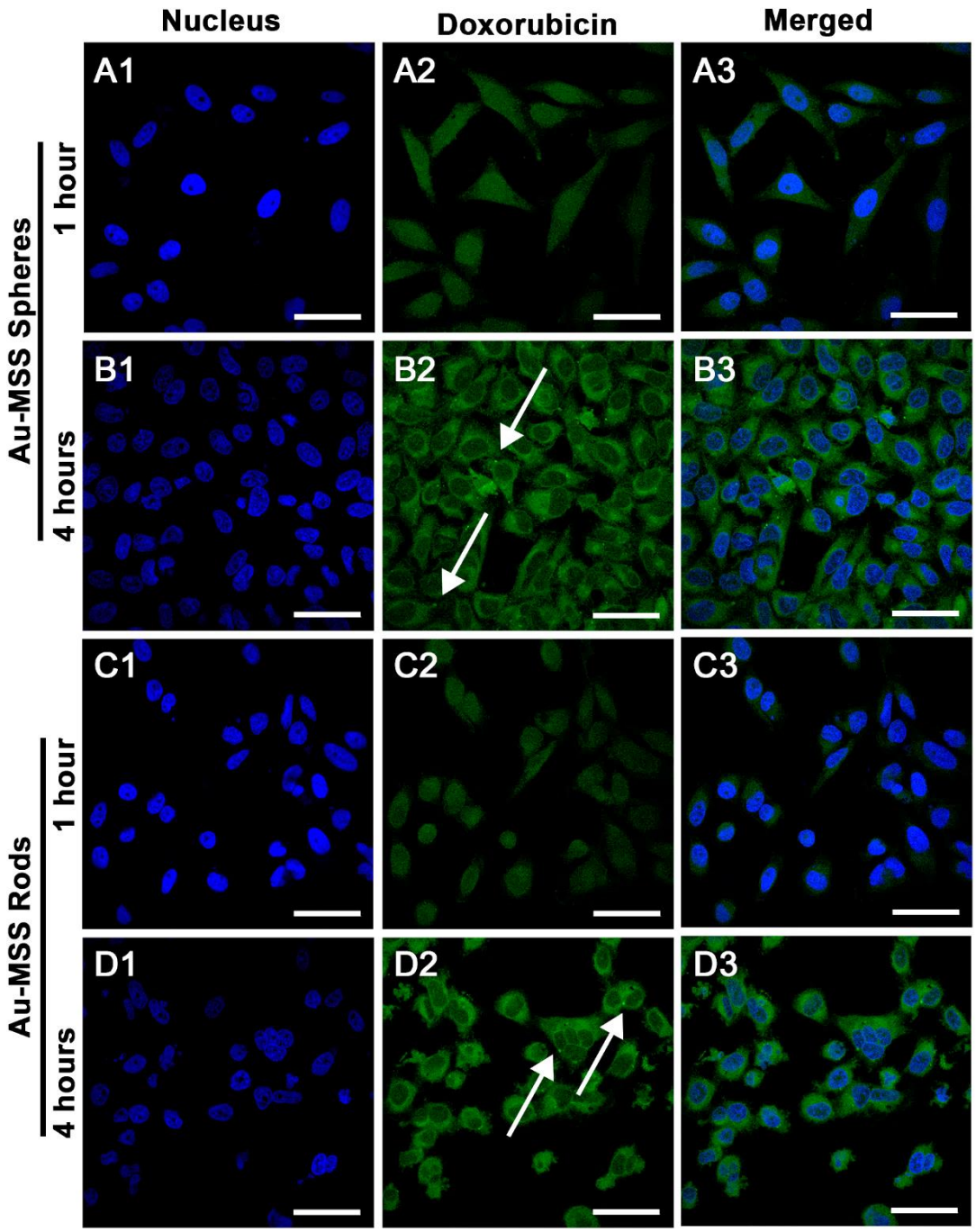

Figure 20 - Confocal microscopy images of Dox loaded Au-MSSs uptake by HeLa cells after 1 and 4 h of incubation. The white arrows are pointing to the internalized nanoparticles. Blue channel: Hoechst 33342® stained cell nucleus; green channel: Dox fluorescence. Scale bar corresponds to 50 µm.

Moreover, when comparing the Dox MFI of the cells treated with Au-MSS rods or spheres (at a concentration of 100 µg/mL) it is possible to observe that Dox MFI is superior for the group treated with Au-MSS rods. Such result may indicate that the Au-MSS rods have a higher cellular internalization than the sphere-shaped particles, which can be explained by the Au-MSS rods higher zeta potential and larger contact area (the longitudinal axis of Au-MSS rods) that favors the particle interaction with the cell membrane particles (Frohlich, 2012, Panariti et al., 2012). Similar findings were also reported by Huang and colleagues for mesoporous silica nanoparticles

with different shapes, where rods with larger aspect ratio presented an increased uptake and a higher internalization rate in A375 cells than the spherical particles (Huang et al., 2010).

Lastly, it is important to notice that the NIR irradiation does not induce the degradation of the Dox molecules or affected the Dox delivery to HeLa cells, since when compared to the non-irradiated groups, no significant differences were observed on Dox MFI.

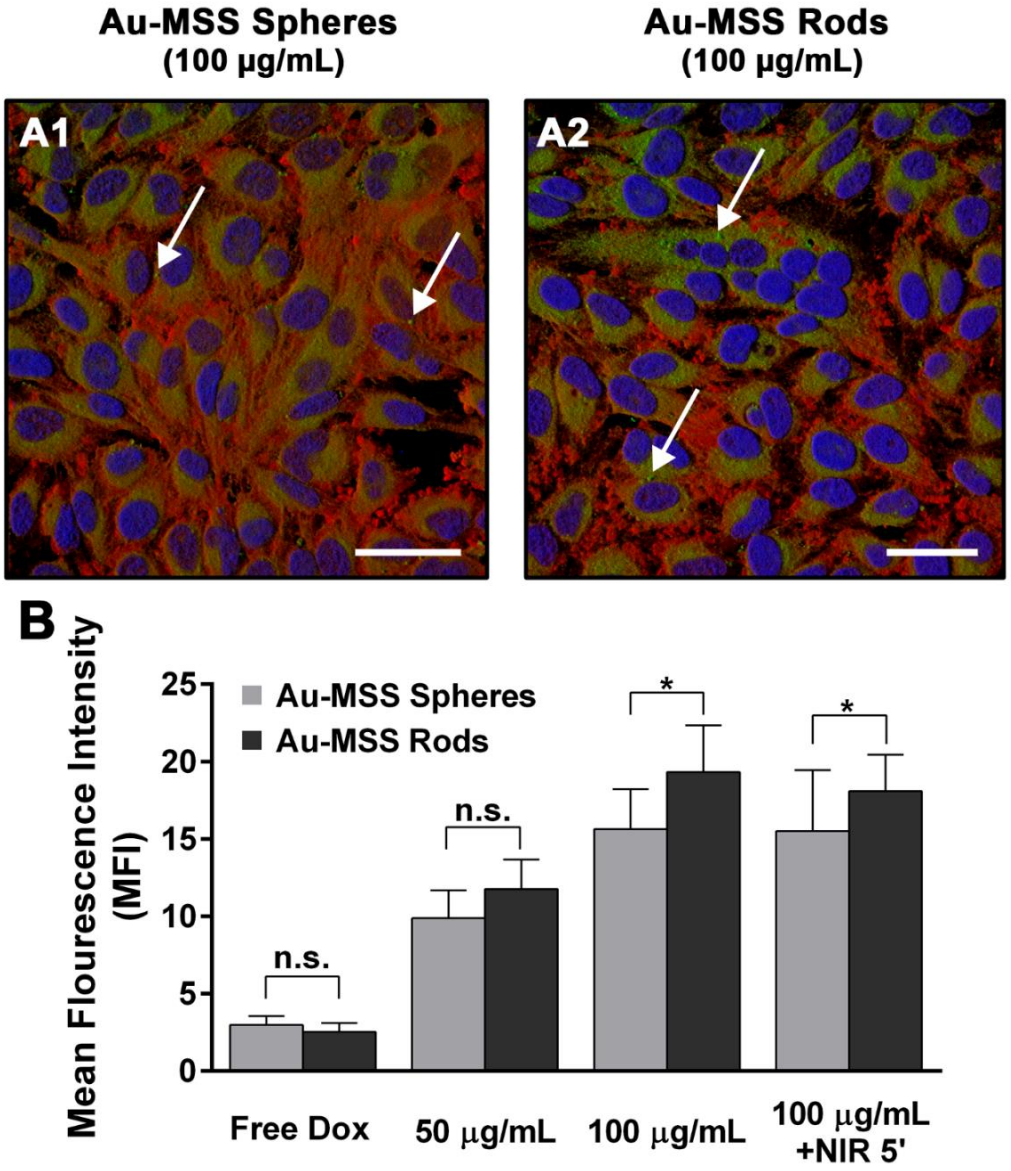

Figure 21 - Analysis of Dox loaded Au-MSSs uptake in HeLa cells after 4 h of incubation. Representative 3D confocal images reconstruction of the Au-MSSs uptake by HeLa cells are presented on (A1) and (A2). The white arrows are pointing to the internalized nanoparticles. Blue channel: Hoechst 33342® stained cell nucleus; Red channel: WGA-Alexa Fluor® 594 conjugate for cell cytoplasm staining; Green channel: Dox fluorescence. (B) Analysis of mean fluorescence intensity of Dox at 4 h. Scale bar correspond to 50 µm. Data are presented as mean ± s.d., *p<0,05, n=20.

3.9. Characterization of the cytotoxic profile of the nanoparticles

In order to evaluate the therapeutic potential of Dox-loaded Au-MSS spheres or rods, their cytotoxic activity towards HeLa cells was assessed. HeLa cells were incubated with various concentrations of nanoparticle formulations, i.e., 20 (with 2.8 μM of loaded Dox), 60 (with 8.3 μM of loaded Dox) and 100 μg/mL (with 13.8 μM of loaded Dox) with or without NIR laser irradiation, or similar free DOX concentrations (Figure 22 A).

As depicted in Figure 22 (B, C, and D), the different Au-MSS formulations led to a decrease in cell viability that is proportional to the tested concentrations of Au-MSSs. Moreover, in general, all the Au-MSS formulations induced a higher cytotoxicity than the free drug counterparts, which may be the result of the increased capacity of Au-MSSs to deliver Dox to HeLa cells as previously observed in uptake studies (section 3.8.). Furthermore, the Au-MSS spheres and rods, in the absence of NIR irradiation, presented a similar cytotoxic effect (i.e. ~40, 30 and 15% for concentrations of 20, 60 and 100 μg/mL, respectively). However, it is important to notice that the Au-MSS rods possess a lower drug encapsulation efficiency and therefore a lower quantity of Dox per nanoparticle. This similar cytotoxic effect may be justified by the increased cellular internalization observed for Au-MSS rods when compared to the spherical counterparts. On the other side, when cells were exposed to NIR irradiation, the Au-MSS rods at concentrations of 60 and 100 μg/mL presented an enhanced cytotoxic effect (only 24% and 7% of cells remained viable, respectively) when compared to the spheres, (26% and 20%). Such clearly demonstrates that the NIR irradiation and consequent heat production can improve the carrier cytotoxic effect by sensitizing the HeLa cells to Dox action or even by promoting cell death. The Au-MSS spheres exposition to the NIR irradiation did not elicit any significant variation on the cytotoxic effect, due to their low photothermal properties, which is in accordance with the data reported in literature, where similar Au-MSSs approaches were used (Tang et al., 2012, Zhang et al., 2015). Zhang and colleagues prepared gold-silica-based NRs with Dox grafted (chemical linkage/bond) onto the pore of MSS. In their work, the drug delivery without NIR exposition led to a decrease in cell viability up to 50%. However, when the particles were incubated and irradiated with NIR laser for 5 min, the cell viability decreased to about 30% due to the heat generation (Zhang et al., 2015). Relatively to the sphere shaped Au-MSS systems, their application for drug delivery to cancer cells has been poorly explored with no significant data being found in literature, since this type of Au-MSSs is mainly studied for imaging-related applications.

From a therapeutic point of view, the chemo- and thermo- therapy combination can be a crucial factor to improve the cancer treatment by acting simultaneously on different cancer cell hallmarks and by modulating the particle effect upon NIR laser irradiation, in order to originate a synergistic antitumoral effect capable of eradicating the tumor without eliciting any side effects.

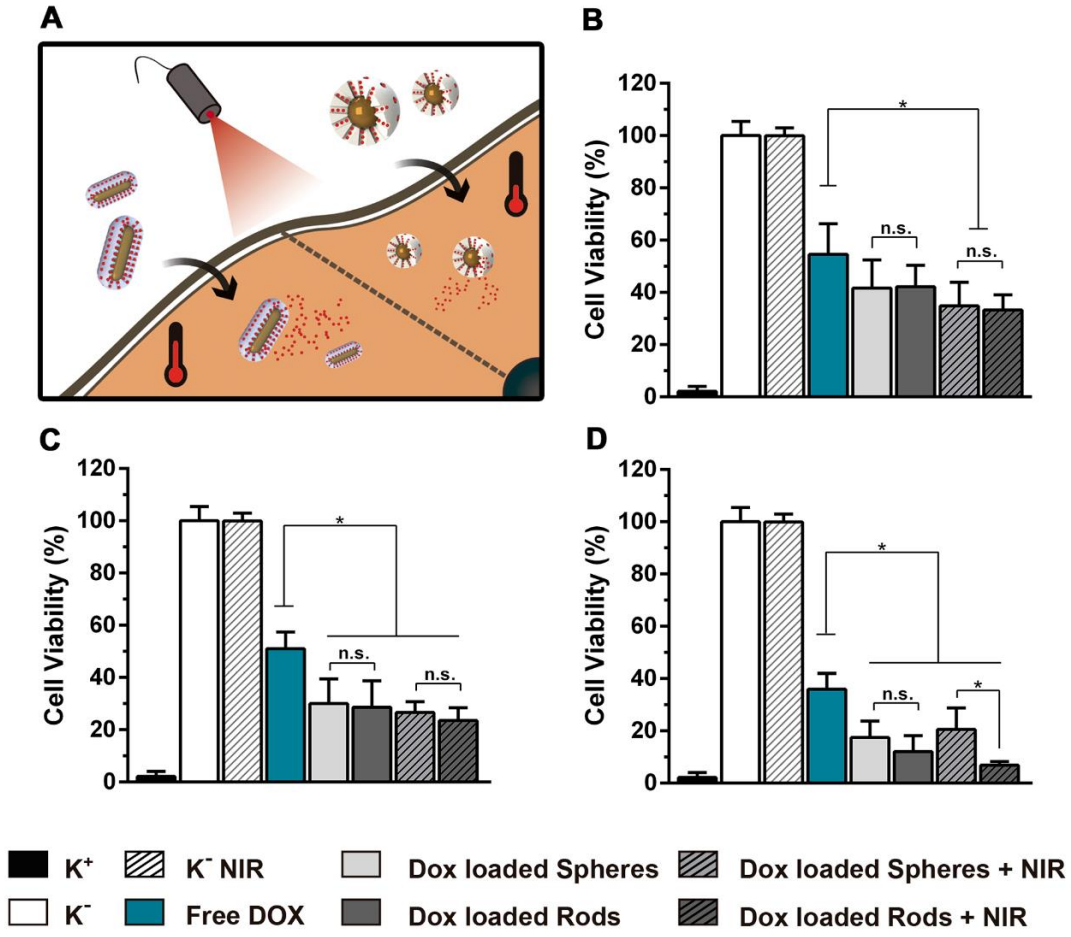

Figure 22 - Cytotoxic effect of Dox loaded Au-MSS nanoparticles in HeLa cells. (A) Schematic representation of Au-MSSs cytotoxic activity upon NIR irradiation (808 nm, 1.7 W/cm^2, 5 min). Cytotoxic activity of Au-MSSs at concentrations of (B) 20, (C) 60, and (D) 100 μg/mL. K^+: cells treated with ethanol. (K^-): non-treated HeLa cells and (K^- NIR): non-treated HeLa cells upon NIR irradiation (808 nm, 1.7 W/cm^2, 5 min). Data are represented as mean ± s.d., *p<0.05, n=5.

Chapter 4

Conclusion and Future Perspectives

4. Conclusion and Future Perspectives

The application of Nanotechnology in Medicine has grown in the past years, and a particular focus has been given to cancer-related issues. The cancer conventional therapies present several limitations such as their weak specificity and their severe side effects. The use of nanoparticles in cancer therapy has been regarded as being an advantageous approach capable of improving the pharmacokinetic profile of the therapeutic agents. Moreover, the nanocarriers design is an important parameter that influences their performance in biological environments. Among the different particle parameters, the nanomaterials shape has a high impact on the nanoparticles interaction with cells and on the therapeutic efficacy, however, this feature has been poorly explored in the literature.

In this thesis, rod- and sphere-shaped nanoparticles, composed of a gold core coated with mesoporous silica, were produced in order to study the effect of nanomaterials shape on their biological performance, namely on the biocompatibility, cellular uptake and cytotoxic activity. Herein, the obtained results revealed that both Au-MSSs displayed suitable sizes, allowing them to take advantage of the EPR effect. Furthermore, the Au-MSS rods presented an UV-vis absorption peak at 770 nm (not present in Au-MSS with spherical shape), which make these particles adequate for being applied in PTT. On the other side, the spherical Au-MSS were capable of encapsulating a higher payload of Dox, displaying an encapsulation efficiency around 80%, whereas the rod-like particles only encapsulated 52% of the Dox. Further, Au-MSS rods were capable of delivering higher quantities of Dox to the cancer cells when compared to the spherical counterparts, which indicates that these rod-like particles are more internalized by cancer cells. In the cytotoxic studies, both Au-MSSs presented an enhanced cytotoxicity activity when compared to the free Dox administration. Moreover, Au-MSS rods without NIR laser irradiation were capable of inducing a similar cytotoxic effect to that of spherical particles, even carrying a lower Dox amount. Further, the NIR laser irradiation was also capable of potentiating the cytotoxic effect of Au-MSS rods, thus indicating that the generated heat sensitizes the cells to the Dox action or induces cell death. Moreover, it is important to notice that the Au-MSS spheres application in drug delivery for cancer therapy has been poorly explored, since no significant data is available in literature. So far, Au-MSS spheres were mainly used for imaging-related applications.

In the future, the versatility of Au-MSSs to encapsulate both hydrophilic and hydrophobic drugs and the possibility to combine their delivery with the PTT can be explored to develop multifunctional platforms. Furthermore, the heat generation can also be used to promote a stimuli responsive drug delivery by functionalizing the particle surface with thermoresponsive moieties, such as DNA, Poly(N-isopropylacrylamide) (PNIPAM) and cucurbit[6]uril. Moreover, the inclusion of cancer cell targeting biomolecules on MSS surface will be critical for improving

cancer treatments selectivity. In addition, both Au-MSSs have the potential to be used as imaging agents which further expands their applicability in the biomedical area.

Chapter 5

References

5. References

Abadeer, N. S. and Murphy, C. J. (2016). "Recent Progress in Cancer Thermal Therapy Using Gold Nanoparticles." The Journal of Physical Chemistry C, 120: 4691-4716.

Ahmed, S., Annu, Ikram, S. and Yudha, S. S. (2016). "Biosynthesis of gold nanoparticles: A green approach." Journal of Photochemistry and Photobiology B: Biology, 161: 141-153.

Akbarzadeh, A., Rezaei-Sadabady, R., Davaran, S., Joo, S. W., Zarghami, N., Hanifehpour, Y., Samiei, M., Kouhi, M. and Nejati-Koshki, K. (2013). "Liposome: classification, preparation, and applications." Nanoscale Research Letters, 8: 102.

Akhter, S., Ahmad, M. Z., Ahmad, F. J., Storm, G. and Kok, R. J. (2012). "Gold nanoparticles in theranostic oncology: current state-of-the-art." Expert Opinion on Drug Delivery, 9: 1225-1243.

Albanese, A., Tang, P. S. and Chan, W. C. (2012). "The effect of nanoparticle size, shape, and surface chemistry on biological systems." Annual Review of Biomedical Engineering, 14: 1-16.

Alex, S. and Tiwari, A. (2015). "Functionalized Gold Nanoparticles: Synthesis, Properties and Applications--A Review." Journal of Nanoscience and Nanotechnology, 15: 1869-1894.

Alkilany, A. M., Lohse, S. E. and Murphy, C. J. (2013). "The gold standard: gold nanoparticle libraries to understand the nano-bio interface." Accounts of Chemical Research, 46: 650-661.

Alkilany, A. M., Nagaria, P. K., Hexel, C. R., Shaw, T. J., Murphy, C. J. and Wyatt, M. D. (2009). "Cellular uptake and cytotoxicity of gold nanorods: molecular origin of cytotoxicity and surface effects." Small, 5: 701-708.

ALOthman, Z. A. (2012). "A review: fundamental aspects of silicate mesoporous materials." Materials, 5: 2874-2902.

Amoozgar, Z. and Yeo, Y. (2012). "Recent advances in stealth coating of nanoparticle drug delivery systems." Wiley Interdisciplinary Reviews: Nanomedicine and Nanobiotechnology, 4: 219-233.

Arami, H., Khandhar, A., Liggitt, D. and Krishnan, K. M. (2015). "In vivo delivery, pharmacokinetics, biodistribution and toxicity of iron oxide nanoparticles." Chemical Society Reviews, 44: 8576-8607.

Artandi, S. E. and DePinho, R. A. (2010). "Telomeres and telomerase in cancer." Carcinogenesis, 31: 9-18.

Bao, C., Conde, J., Polo, E., del Pino, P., Moros, M., Baptista, P. V., Grazu, V., Cui, D. and de la Fuente, J. M. (2014). "A promising road with challenges: where are gold nanoparticles in translational research?" Nanomedicine, 9: 2353-2370.

Bertrand, N., Wu, J., Xu, X., Kamaly, N. and Farokhzad, O. C. (2014). "Cancer nanotechnology: the impact of passive and active targeting in the era of modern cancer biology." Advanced Drug Delivery Reviews, 66: 2-25.

Black, K. C., Wang, Y., Luehmann, H. P., Cai, X., Xing, W., Pang, B., Zhao, Y., Cutler, C. S., Wang, L. V. and Liu, Y. (2014). "Radioactive 198Au-doped nanostructures with different shapes for in vivo analyses of their biodistribution, tumor uptake, and intratumoral distribution." ACS Nano, 8: 4385-4394.

Blanco, E., Shen, H. and Ferrari, M. (2015). "Principles of nanoparticle design for overcoming biological barriers to drug delivery." Nature Biotechnology, 33: 941-951.

Breier, A., Gibalova, L., Seres, M., Barancik, M. and Sulova, Z. (2013). "New insight into p-glycoprotein as a drug target." Anti-cancer Agents in Medicinal Chemistry, 13: 159-170.

Champion, J. A. and Mitragotri, S. (2009). "Shape induced inhibition of phagocytosis of polymer particles." Pharmaceutical Research, 26: 244-249.

Chatterjee, D. K., Diagaradjane, P. and Krishnan, S. (2011). "Nanoparticle-mediated hyperthermia in cancer therapy." Therapeutic Delivery, 2: 1001-1014.

Chen, J., Zhang, R., Han, L., Tu, B. and Zhao, D. (2013). "One-pot synthesis of thermally stable gold@ mesoporous silica core-shell nanospheres with catalytic activity." Nano Research, 6: 871-879.

Chen, Y., Wang, Q. and Wang, T. (2015). "Facile large-scale synthesis of brain-like mesoporous silica nanocomposites via a selective etching process." Nanoscale, 7: 16442-16450.

Chen, Y. S., Frey, W., Kim, S., Homan, K., Kruizinga, P., Sokolov, K. and Emelianov, S. (2010). "Enhanced thermal stability of silica-coated gold nanorods for photoacoustic imaging and image-guided therapy." Optics Express, 18: 8867-8878.

Chu, K. F. and Dupuy, D. E. (2014). "Thermal ablation of tumours: biological mechanisms and advances in therapy." Nature Reviews Cancer, 14: 199-208.

Cobley, C. M., Chen, J., Cho, E. C., Wang, L. V. and Xia, Y. (2011). "Gold nanostructures: a class of multifunctional materials for biomedical applications." Chemical Society Reviews, 40: 44-56.

Cole, L. E., Ross, R. D., Tilley, J. M., Vargo-Gogola, T. and Roeder, R. K. (2015). "Gold nanoparticles as contrast agents in x-ray imaging and computed tomography." Nanomedicine: Nanotechnology, Biology, and Medicine, 10: 321-341.

de Melo-Diogo, D., Gaspar, V. M., Costa, E. C., Moreira, A. F., Oppolzer, D., Gallardo, E. and Correia, I. J. (2014). "Combinatorial delivery of Crizotinib–Palbociclib–Sildenafil using TPGS-PLA micelles for improved cancer treatment." European Journal of Pharmaceutics and Biopharmaceutics, 88: 718-729.

DeSantis, C. E., Lin, C. C., Mariotto, A. B., Siegel, R. L., Stein, K. D., Kramer, J. L., Alteri, R., Robbins, A. S. and Jemal, A. (2014). "Cancer treatment and survivorship statistics, 2014." CA: a Cancer Journal for Clinicians, 64: 252-271.

Dhumale, V. A., Gangwar, R. K., Datar, S. S. and Sharma, R. B. (2012). "Reversible aggregation control of polyvinylpyrrolidone capped gold nanoparticles as a function of pH." Materials Express, 2: 311-318.

Ding, Y., Zhou, Y. Y., Chen, H., Geng, D. D., Wu, D. Y., Hong, J., Shen, W. B., Hang, T. J. and Zhang, C. (2013). "The performance of thiol-terminated PEG-paclitaxel-conjugated gold nanoparticles." Biomaterials, 34: 10217-10227.

Dong, X. and Mumper, R. J. (2010). "Nanomedicinal strategies to treat multidrug-resistant tumors: current progress." Nanomedicine, 5: 597-615.

Dreaden, E. C., Alkilany, A. M., Huang, X., Murphy, C. J. and El-Sayed, M. A. (2012). "The golden age: gold nanoparticles for biomedicine." Chemical Society Reviews, 41: 2740-2779.

Elsabahy, M. and Wooley, K. L. (2012). "Design of polymeric nanoparticles for biomedical delivery applications." Chemical Society Reviews, 41: 2545-2561.

Ernsting, M. J., Murakami, M., Roy, A. and Li, S. D. (2013). "Factors controlling the pharmacokinetics, biodistribution and intratumoral penetration of nanoparticles." Journal of Controlled Release, 172: 782-794.

Farokhzad, O. C. and Langer, R. (2009). "Impact of nanotechnology on drug delivery." ACS Nano, 3: 16-20.

Floor, S. L., Dumont, J. E., Maenhaut, C. and Raspe, E. (2012). "Hallmarks of cancer: of all cancer cells, all the time?" Trends in Molecular Medicine, 18: 509-515.

Frens, G. (1973). "Controlled nucleation for the regulation of the particle size in monodisperse gold suspensions." Nature, 241: 20-22.

Frohlich, E. (2012). "The role of surface charge in cellular uptake and cytotoxicity of medical nanoparticles." International Journal of Nanomedicine, 7: 5577-5591.

Gao, J., Huang, X., Liu, H., Zan, F. and Ren, J. (2012). "Colloidal stability of gold nanoparticles modified with thiol compounds: bioconjugation and application in cancer cell imaging." Langmuir, 28: 4464-4471.

Gaspar, V. M., Moreira, A. F., Costa, E. C., Queiroz, J. A., Sousa, F., Pichon, C. and Correia, I. J. (2015). "Gas-generating TPGS-PLGA microspheres loaded with nanoparticles (NIMPS) for co-delivery of minicircle DNA and anti-tumoral drugs." Colloids and Surfaces. B, Biointerfaces, 134: 287-294.

Gautier, J., Allard-Vannier, E., Herve-Aubert, K., Souce, M. and Chourpa, I. (2013). "Design strategies of hybrid metallic nanoparticles for theragnostic applications." Nanotechnology, 24: 432002.

Ghosh Chaudhuri, R. and Paria, S. (2012). "Core/shell nanoparticles: classes, properties, synthesis mechanisms, characterization, and applications." Chemical Reviews, 112: 2373-2433.

Giampazolias, E. and Tait, S. W. (2016). "Mitochondria and the hallmarks of cancer." The FEBS Journal, 283: 803-814.

Goel, H. L. and Mercurio, A. M. (2013). "VEGF targets the tumour cell." Nature Reviews Cancer, 13: 871-882.

Gorelikov, I. and Matsuura, N. (2008). "Single-step coating of mesoporous silica on cetyltrimethyl ammonium bromide-capped nanoparticles." Nano Letters, 8: 369-373.

Gupta, A., Moyano, D. F., Parnsubsakul, A., Papadopoulos, A., Wang, L.-S., Landis, R. F., Das, R. and Rotello, V. M. (2016). "Ultra-stable Biofunctionalizable Gold Nanoparticles." ACS Applied Materials & Interfaces, 8: 14096–14101.

Hanahan, D. and Coussens, L. M. (2012). "Accessories to the crime: functions of cells recruited to the tumor microenvironment." Cancer Cell, 21: 309-322.

Hanahan, D. and Weinberg, R. A. (2000). "The hallmarks of cancer." Cell, 100: 57-70.

Hanahan, D. and Weinberg, R. A. (2011). "Hallmarks of cancer: the next generation." Cell, 144: 646-674.

Heo, J. H., Kim, K. I., Cho, H. H., Lee, J. W., Lee, B. S., Yoon, S., Park, K. J., Lee, S., Kim, J., Whang, D. and Lee, J. H. (2015). "Ultrastable-Stealth Large Gold Nanoparticles with DNA Directed Biological Functionality." Langmuir, 31: 13773-13782.

Holohan, C., Van Schaeybroeck, S., Longley, D. B. and Johnston, P. G. (2013). "Cancer drug resistance: an evolving paradigm." Nature Reviews Cancer, 13: 714-726.

Hoshyar, N., Gray, S., Han, H. and Bao, G. (2016). "The effect of nanoparticle size on in vivo pharmacokinetics and cellular interaction." Nanomedicine, 11: 673-692.

Hu, Q., Sun, W., Wang, C. and Gu, Z. (2016). "Recent advances of cocktail chemotherapy by combination drug delivery systems." Advanced Drug Delivery Reviews, 98: 19-34.

Huang, H. C., Barua, S., Sharma, G., Dey, S. K. and Rege, K. (2011). "Inorganic nanoparticles for cancer imaging and therapy." Journal of Controlled Release, 155: 344-357.

Huang, X., El-Sayed, I. H., Qian, W. and El-Sayed, M. A. (2006). "Cancer cell imaging and photothermal therapy in the near-infrared region by using gold nanorods." Journal of the American Chemical Society, 128: 2115-2120.

Huang, X. and El-Sayed, M. A. (2010). "Gold nanoparticles: Optical properties and implementations in cancer diagnosis and photothermal therapy." Journal of Advanced Research, 1: 13-28.

Huang, X., Jain, P. K., El-Sayed, I. H. and El-Sayed, M. A. (2008). "Plasmonic photothermal therapy (PPTT) using gold nanoparticles." Lasers in Medical Science, 23: 217-228.

Huang, X., Teng, X., Chen, D., Tang, F. and He, J. (2010). "The effect of the shape of mesoporous silica nanoparticles on cellular uptake and cell function." Biomaterials, 31: 438-448.

Issels, R. D. (2008). "Hyperthermia adds to chemotherapy." European Journal of Cancer, 44: 2546-2554.

Jain, P. K., Lee, K. S., El-Sayed, I. H. and El-Sayed, M. A. (2006). "Calculated absorption and scattering properties of gold nanoparticles of different size, shape, and composition: applications in biological imaging and biomedicine." The Journal of Physical Chemistry. B, 110: 7238-7248.

Jain, S., Hirst, D. and O'Sullivan, J. (2012). "Gold nanoparticles as novel agents for cancer therapy." The British Journal of Radiology, 85: 101-113.

Jalani, G. and Cerruti, M. (2015). "Nano graphene oxide-wrapped gold nanostars as ultrasensitive and stable SERS nanoprobes." Nanoscale, 7: 9990-9997.

Janát-Amsbury, M., Ray, A., Peterson, C. and Ghandehari, H. (2011). "Geometry and surface characteristics of gold nanoparticles influence their biodistribution and uptake by macrophages." European Journal of Pharmaceutics and Biopharmaceutics, 77: 417-423.

Jemal, A., Bray, F., Center, M. M., Ferlay, J., Ward, E. and Forman, D. (2011). "Global cancer statistics." CA: a Cancer Journal for Clinicians, 61: 69-90.

Jia, F., Liu, X., Li, L., Mallapragada, S., Narasimhan, B. and Wang, Q. (2013a). "Multifunctional nanoparticles for targeted delivery of immune activating and cancer therapeutic agents." Journal of Controlled Release, 172: 1020-1034.

Jia, L., Shen, J., Li, Z., Zhang, D., Zhang, Q., Liu, G., Zheng, D. and Tian, X. (2013b). "In vitro and in vivo evaluation of paclitaxel-loaded mesoporous silica nanoparticles with three pore sizes." International Journal of Pharmaceutics, 445: 12-19.

Joyce, J. A. and Pollard, J. W. (2009). "Microenvironmental regulation of metastasis." Nature Reviews Cancer, 9: 239-252.

Kanehara, M., Watanabe, Y. and Teranishi, T. (2009). "Thermally stable silica-coated hydrophobic gold nanoparticles." Journal of Nanoscience and Nanotechnology, 9: 673-675.

Kango, S., Kalia, S., Celli, A., Njuguna, J., Habibi, Y. and Kumar, R. (2013). "Surface modification of inorganic nanoparticles for development of organic–inorganic nanocomposites—a review." Progress in Polymer Science, 38: 1232-1261.

Kelly, G. L. and Strasser, A. (2011). "The essential role of evasion from cell death in cancer." Advances in Cancer Research, 111: 39-96.

Kemp, J. A., Shim, M. S., Heo, C. Y. and Kwon, Y. J. (2016). ""Combo" nanomedicine: Co-delivery of multi-modal therapeutics for efficient, targeted, and safe cancer therapy." Advanced Drug Delivery Reviews, 98: 3-18.

Krishnan, S., Diagaradjane, P. and Cho, S. H. (2010). "Nanoparticle-mediated thermal therapy: evolving strategies for prostate cancer therapy." International Journal of Hyperthermia, 26: 775-789.

Kumari, P., Ghosh, B. and Biswas, S. (2016). "Nanocarriers for cancer-targeted drug delivery." Journal of Drug Targeting, 24: 179-191.

Li, X., Zhi, C., Hanagata, N., Yamaguchi, M., Bando, Y. and Golberg, D. (2013). "Boron nitride nanotubes functionalized with mesoporous silica for intracellular delivery of chemotherapy drugs." Chemical Communications, 49: 7337-7339.

Lila, A. S. A., Nawata, K., Shimizu, T., Ishida, T. and Kiwada, H. (2013). "Use of polyglycerol (PG), instead of polyethylene glycol (PEG), prevents induction of the accelerated blood clearance phenomenon against long-circulating liposomes upon repeated administration." International Journal of Pharmaceutics, 456: 235-242.

Liu, B., Li, C., Cheng, Z., Hou, Z., Huang, S. and Lin, J. (2016). "Functional nanomaterials for near-infrared-triggered cancer therapy." Biomaterials Science, 4: 890-909.

Liu, J., Detrembleur, C., Pauw-Gillet, D., Mornet, S., Jérôme, C. and Duguet, E. (2015a). "Gold Nanorods Coated with Mesoporous Silica Shell as Drug Delivery System for Remote Near Infrared Light-Activated Release and Potential Phototherapy." Small, 11: 2323-2332.

Liu, J. N., Bu, W. B. and Shi, J. L. (2015b). "Silica coated upconversion nanoparticles: a versatile platform for the development of efficient theranostics." Accounts of Chemical Research, 48: 1797-1805.

Liu, Y., Xu, M., Chen, Q., Guan, G., Hu, W., Zhao, X., Qiao, M., Hu, H., Liang, Y. and Zhu, H. (2015c). "Gold nanorods/mesoporous silica-based nanocomposite as theranostic agents for targeting near-infrared imaging and photothermal therapy induced with laser." International Journal of Nanomedicine, 10: 4747-4761.

Luo, G. F., Chen, W. H., Liu, Y., Lei, Q., Zhuo, R. X. and Zhang, X. Z. (2014). "Multifunctional enveloped mesoporous silica nanoparticles for subcellular co-delivery of drug and therapeutic peptide." Scientific Reports, 4: 6064.

Madani, S. Y., Naderi, N., Dissanayake, O., Tan, A. and Seifalian, A. M. (2011). "A new era of cancer treatment: carbon nanotubes as drug delivery tools." International Journal of Nanomedicine, 6: 2963-2979.

Maeda, H. (2015). "Toward a full understanding of the EPR effect in primary and metastatic tumors as well as issues related to its heterogeneity." Advanced Drug Delivery Reviews, 91: 3-6.

Maier-Hauff, K., Ulrich, F., Nestler, D., Niehoff, H., Wust, P., Thiesen, B., Orawa, H., Budach, V. and Jordan, A. (2011). "Efficacy and safety of intratumoral thermotherapy using magnetic iron-oxide nanoparticles combined with external beam radiotherapy on patients with recurrent glioblastoma multiforme." Journal of Neuro-Oncology, 103: 317-324.

Mallick, S., Sun, I. C., Kim, K. and Yil, D. K. (2013). "Silica coated gold nanorods for imaging and photo-thermal therapy of cancer cells." Journal of Nanoscience and Nanotechnology, 13: 3223-3229.

Mao, Z., Zhou, X. and Gao, C. (2013). "Influence of structure and properties of colloidal biomaterials on cellular uptake and cell functions." Biomaterials Science, 1: 896-911.

McNeil, S. E. (2009). "Nanoparticle therapeutics: a personal perspective." Wiley Interdisciplinary Reviews: Nanomedicine and Nanobiotechnology, 1: 264-271.

Mekaru, H., Lu, J. and Tamanoi, F. (2015). "Development of mesoporous silica-based nanoparticles with controlled release capability for cancer therapy." Advanced Drug Delivery Reviews, 95: 40-49.

Miranda, N., Portugal, C., Nogueira, P. J., Farinha, C. S., Oliveira, A. L., Soares, A. P., Alves, M. I., Martins, J., Mendanha, T., Rosa, M. V., Silva, C. and Serra, L. (2015). Portugal - Doenças Oncológicas em Números – 2015. Lisboa.

Mitragotri, S., Burke, P. A. and Langer, R. (2014). "Overcoming the challenges in administering biopharmaceuticals: formulation and delivery strategies." Nature Reviews Drug Discovery, 13: 655-672.

Moreira, A. F., Dias, D. R. and Correia, I. J. (2016). "Stimuli-responsive mesoporous silica nanoparticles for cancer therapy: A review." Microporous and Mesoporous Materials, 236: 141-157.

Moreira, A. F., Gaspar, V. M., Costa, E. C., de Melo-Diogo, D., Machado, P., Paquete, C. M. and Correia, I. J. (2014). "Preparation of end-capped pH-sensitive mesoporous silica nanocarriers for on-demand drug delivery." European Journal of Pharmaceutics and Biopharmaceutics, 88: 1012-1025.

Muddineti, O. S., Ghosh, B. and Biswas, S. (2015). "Current trends in using polymer coated gold nanoparticles for cancer therapy." International Journal of Pharmaceutics, 484: 252-267.

Nazir, S., Hussain, T., Ayub, A., Rashid, U. and MacRobert, A. J. (2014). "Nanomaterials in combating cancer: therapeutic applications and developments." Nanomedicine: Nanotechnology, Biology, and Medicine, 10: 19-34.

Nicol, J. R., Dixon, D. and Coulter, J. A. (2015). "Gold nanoparticle surface functionalization: a necessary requirement in the development of novel nanotherapeutics." Nanomedicine, 10: 1315-1326.

Niidome, T., Yamagata, M., Okamoto, Y., Akiyama, Y., Takahashi, H., Kawano, T., Katayama, Y. and Niidome, Y. (2006). "PEG-modified gold nanorods with a stealth character for in vivo applications." Journal of Controlled Release, 114: 343-347.

Nikoobakht, B. and El-Sayed, M. A. (2003). "Preparation and growth mechanism of gold nanorods (NRs) using seed-mediated growth method." Chemistry of Materials, 15: 1957-1962.

Panariti, A., Miserocchi, G. and Rivolta, I. (2012). "The effect of nanoparticle uptake on cellular behavior: disrupting or enabling functions?" Nanotechnology, Science and Applications, 5: 87-100.

Park, K. (2014). "Controlled drug delivery systems: past forward and future back." Journal of Controlled Release, 190: 3-8.

Peer, D., Karp, J. M., Hong, S., Farokhzad, O. C., Margalit, R. and Langer, R. (2007). "Nanocarriers as an emerging platform for cancer therapy." Nature Nanotechnology, 2: 751-760.

Pekkanen, A. M., DeWitt, M. R. and Rylander, M. N. (2014). "Nanoparticle enhanced optical imaging and phototherapy of cancer." Journal of Biomedical Nanotechnology, 10: 1677-1712.

Perala, S. R. and Kumar, S. (2013). "On the mechanism of metal nanoparticle synthesis in the Brust-Schiffrin method." Langmuir, 29: 9863-9873.

Pérez-Juste, J., Pastoriza-Santos, I., Liz-Marzán, L. M. and Mulvaney, P. (2005). "Gold nanorods: synthesis, characterization and applications." Coordination Chemistry Reviews, 249: 1870-1901.

Petros, R. A. and DeSimone, J. M. (2010). "Strategies in the design of nanoparticles for therapeutic applications." Nature Reviews Drug Discovery, 9: 615-627.

Pickup, M. W., Mouw, J. K. and Weaver, V. M. (2014). "The extracellular matrix modulates the hallmarks of cancer." EMBO reports, 15: 1243-1253.

Pietras, K. and Ostman, A. (2010). "Hallmarks of cancer: interactions with the tumor stroma." Experimental Cell Research, 316: 1324-1331.

Quail, D. F. and Joyce, J. A. (2013). "Microenvironmental regulation of tumor progression and metastasis." Nature Medicine, 19: 1423-1437.

Rebucci, M. and Michiels, C. (2013). "Molecular aspects of cancer cell resistance to chemotherapy." Biochemical Pharmacology, 85: 1219-1226.

Reuveni, T., Motiei, M., Romman, Z., Popovtzer, A. and Popovtzer, R. (2011). "Targeted gold nanoparticles enable molecular CT imaging of cancer: an in vivo study." International Journal of Nanomedicine, 6: 2859-2864.

Ribeiro, M. P., Espiga, A., Silva, D., Baptista, P., Henriques, J., Ferreira, C., Silva, J. C., Borges, J. P., Pires, E., Chaves, P. and Correia, I. J. (2009). "Development of a new chitosan hydrogel for wound dressing." Wound Repair and Regeneration, 17: 817-824.

Rocha-Santos, T. A. (2014). "Sensors and biosensors based on magnetic nanoparticles." TrAC Trends in Analytical Chemistry, 62: 28-36.

Ruff, J., Steitz, J., Buchkremer, A., Noyong, M., Hartmann, H., Besmehn, A. and Simon, U. (2016). "Multivalency of PEG-thiol ligands affects the stability of NIR-absorbing hollow gold nanospheres and gold nanorods." Journal of Materials Chemistry B, 4: 2828-2841.

Sadeghnia, H. R., Zoljalali, N., Hanafi-Bojd, M. Y., Nikoofal-Sahlabadi, S. and Malaekeh-Nikouei, B. (2015). "Effect of mesoporous silica nanoparticles on cell viability and markers of oxidative stress." Toxicology Mechanisms and Methods, 25: 433-439.

Sagnella, S. M., McCarroll, J. A. and Kavallaris, M. (2014). "Drug delivery: beyond active tumour targeting." Nanomedicine: Nanotechnology, Biology, and Medicine, 10: 1131-1137.

Sahay, G., Alakhova, D. Y. and Kabanov, A. V. (2010). "Endocytosis of nanomedicines." Journal of Controlled Release, 145: 182-195.

Sasidharan, A. and Monteiro-Riviere, N. A. (2015). "Biomedical applications of gold nanomaterials: opportunities and challenges." Wiley Interdisciplinary Reviews: Nanomedicine and Nanobiotechnology, 7: 779-796.

Scarabelli, L., Sa□nchez-Iglesias, A., Pe□rez-Juste, J. and Liz-Marza□n, L. M. (2015). "A "Tips and Tricks" Practical Guide to the Synthesis of Gold Nanorods." The Journal of Physical Chemistry Letters, 6: 4270-4279.

Schneider, C. A., Rasband, W. S. and Eliceiri, K. W. (2012). "NIH Image to ImageJ: 25 years of image analysis." Nature Methods, 9: 671-675.

Sharif, F. (2012). "Mesoporous silica nanoparticles as a compound delivery system in zebrafish embryos." International Journal of Nanomedicine, 7: 1875-1890.

Shen, S., Tang, H., Zhang, X., Ren, J., Pang, Z., Wang, D., Gao, H., Qian, Y., Jiang, X. and Yang, W. (2013). "Targeting mesoporous silica-encapsulated gold nanorods for chemo-photothermal therapy with near-infrared radiation." Biomaterials, 34: 3150-3158.

Siegel, R. L., Miller, K. D. and Jemal, A. (2015). "Cancer statistics, 2015." CA: a Cancer Journal for Clinicians, 65: 5-29.

Siepmann, J. and Siepmann, F. (2008). "Mathematical modeling of drug delivery." International Journal of Pharmaceutics, 364: 328-343.

Song, J. T., Yang, X. Q., Zhang, X. S., Yan, D. M., Wang, Z. Y. and Zhao, Y. D. (2015). "Facile Synthesis of Gold Nanospheres Modified by Positively Charged Mesoporous Silica, Loaded with Near-Infrared Fluorescent Dye, for in Vivo X-ray Computed Tomography and Fluorescence Dual Mode Imaging." ACS Applied Materials & Interfaces, 7: 17287-17297.

Sun, T., Zhang, Y. S., Pang, B., Hyun, D. C., Yang, M. and Xia, Y. (2014). "Engineered nanoparticles for drug delivery in cancer therapy." Angewandte Chemie, 53: 12320-12364.

Tang, H., Shen, S., Guo, J., Chang, B., Jiang, X. and Yang, W. (2012). "Gold nanorods@ mSiO 2 with a smart polymer shell responsive to heat/near-infrared light for chemo-photothermal therapy." Journal of Materials Chemistry, 22: 16095-16103.

Tarn, D., Ashley, C. E., Xue, M., Carnes, E. C., Zink, J. I. and Brinker, C. J. (2013). "Mesoporous silica nanoparticle nanocarriers: biofunctionality and biocompatibility." Accounts of Chemical Research, 46: 792-801.

Tong, R. and Kohane, D. S. (2016). "New Strategies in Cancer Nanomedicine." Annual Review of Pharmacology and Toxicology, 56: 41-57.

Torre, L. A., Bray, F., Siegel, R. L., Ferlay, J., Lortet-Tieulent, J. and Jemal, A. (2015). "Global cancer statistics, 2012." CA: a Cancer Journal for Clinicians, 65: 87-108.

Turkevich, J., Stevenson, P. C. and Hillier, J. (1951). "A study of the nucleation and growth processes in the synthesis of colloidal gold." Discussions of the Faraday Society, 11: 55-75.

Versiani, A. F., Andrade, L. M., Martins, E. M., Scalzo, S., Geraldo, J. M., Chaves, C. R., Ferreira, D. C., Ladeira, M., Guatimosim, S. and Ladeira, L. O. (2016). "Gold nanoparticles and their applications in biomedicine." Future Virology, 11: 293-309.

Vogel, A. and Venugopalan, V. (2003). "Mechanisms of pulsed laser ablation of biological tissues." Chemical Reviews, 103: 577-644.

Wang, A. Z., Langer, R. and Farokhzad, O. C. (2012a). "Nanoparticle delivery of cancer drugs." Annual Review of Medicine, 63: 185-198.

Wang, J., Zhu, G., You, M., Song, E., Shukoor, M. I., Zhang, K., Altman, M. B., Chen, Y., Zhu, Z., Huang, C. Z. and Tan, W. (2012b). "Assembly of aptamer switch probes and photosensitizer on gold nanorods for targeted photothermal and photodynamic cancer therapy." ACS Nano, 6: 5070-5077.

Wang, S. (2009). "Ordered mesoporous materials for drug delivery." Microporous and Mesoporous Materials, 117: 1-9.

Wang, Y., Black, K. C., Luehmann, H., Li, W., Zhang, Y., Cai, X., Wan, D., Liu, S. Y., Li, M., Kim, P., Li, Z. Y., Wang, L. V., Liu, Y. and Xia, Y. (2013). "Comparison study of gold nanohexapods, nanorods, and nanocages for photothermal cancer treatment." ACS Nano, 7: 2068-2077.

Wang, Y., Wang, K., Zhang, R., Liu, X., Yan, X., Wang, J., Wagner, E. and Huang, R. (2014). "Synthesis of core-shell graphitic carbon@silica nanospheres with dual-ordered mesopores for cancer-targeted photothermochemotherapy." ACS Nano, 8: 7870-7879.

Wicki, A., Witzigmann, D., Balasubramanian, V. and Huwyler, J. (2015). "Nanomedicine in cancer therapy: challenges, opportunities, and clinical applications." Journal of Controlled Release, 200: 138-157.

Witsch, E., Sela, M. and Yarden, Y. (2010). "Roles for growth factors in cancer progression." Physiology, 25: 85-101.

Woehrle, G. H., Brown, L. O. and Hutchison, J. E. (2005). "Thiol-functionalized, 1.5-nm gold nanoparticles through ligand exchange reactions: scope and mechanism of ligand exchange." Journal of the American Chemical Society, 127: 2172-2183.

Wu, W. C. and Tracy, J. B. (2015). "Large-Scale Silica Overcoating of Gold Nanorods with Tunable Shell Thicknesses." Chemistry of Materials, 27: 2888-2894.

Xi, D., Dong, S., Meng, X., Lu, Q., Meng, L. and Ye, J. (2012). "Gold nanoparticles as computerized tomography (CT) contrast agents." Royal Society of Chemistry Advances, 2: 12515-12524.

Xu, X., Ho, W., Zhang, X., Bertrand, N. and Farokhzad, O. (2015). "Cancer nanomedicine: from targeted delivery to combination therapy." Trends in Molecular Medicine, 21: 223-232.

Yameen, B., Choi, W. I., Vilos, C., Swami, A., Shi, J. and Farokhzad, O. C. (2014). "Insight into nanoparticle cellular uptake and intracellular targeting." Journal of Controlled Release, 190: 485-499.

Yu, X. and Zhu, Y. (2016). "Preparation of magnetic mesoporous silica nanoparticles as a multifunctional platform for potential drug delivery and hyperthermia." Science and Technology of Advanced Materials, 17: 229-238.

Zeiderman, M. R., Morgan, D. E., Christein, J. D., Grizzle, W. E., McMasters, K. M. and McNally, L. R. (2016). "Acidic pH-Targeted Chitosan-Capped Mesoporous Silica Coated Gold Nanorods Facilitate Detection of Pancreatic Tumors via Multispectral Optoacoustic Tomography." ACS Biomaterials Science & Engineering, 2: 1108-1120.

Zhang, T., Ding, Z., Lin, H., Cui, L., Yang, C., Li, X., Niu, H., An, N., Tong, R. and Qu, F. (2015). "pH-Sensitive Gold Nanorods with a Mesoporous Silica Shell for Drug Release and Photothermal Therapy." European Journal of Inorganic Chemistry, 2015: 2277-2284.

Zhang, Z., Wang, J. and Chen, C. (2013). "Near-infrared light-mediated nanoplatforms for cancer thermo-chemotherapy and optical imaging." Advanced Materials, 25: 3869-3880.

Zhao, P., Li, N. and Astruc, D. (2013). "State of the art in gold nanoparticle synthesis." Coordination Chemistry Reviews, 257: 638-665.

Zou, L., Wang, H., He, B., Zeng, L., Tan, T., Cao, H., He, X., Zhang, Z., Guo, S. and Li, Y. (2016). "Current Approaches of Photothermal Therapy in Treating Cancer Metastasis with Nanotherapeutics." Theranostics, 6: 762-772.

Chapter 6

Appendix

6. Appendix

Moreira, A. F., Dias, D. R., and Correia, I. J. (2016). “Stimuli-responsive mesoporous silica nanoparticles for cancer therapy: A review”. Microporous and Mesoporous Materials. 236: 141-157. (Available on: http://dx.doi.org/10.1016/j.micromeso.2016.08.038)